RARE EARTH AND TRACE ELEMENTS IN AMPHIBOLES OF OCEANIC GABBROS (MARK AREA, MID-ATLANTIC RIDGE) AT MEDIUM- TO LOW-TEMPERATURE SEAFLOOR ALTERATION

Luciano Cortesogno*, Laura Gaggero* and **Alberto Zanetti****

** Dipartimento per lo Studio del Territorio e delle sue Risorse, Università di Genova, Italy (e-mail: cortez@dipteris.unige.it).*
*** CNR - Istituto di Geoscienze e Georisorse di Pavia, Sezione di Pavia, Pavia, Italy.*
Corresponding Author: Laura Gaggero, e-mail gaggero@dipteris.unige.it

Keywords: *metagabbros, rare earths, trace elements, ion microprobe, Mid-Atlantic Ridge.*

ABSTRACT

The gabbro pile cored at the ODP sites 921-924 (Mid-Atlantic Ridge) underwent subseafloor alteration under polyphase retrograde recrystallization from very high temperatures in a ductile deformation regime to amphibolite and greenschist facies under transitional to brittle regimes (Gaggero and Cortesogno, 1997).

To complement the study on the highest grade conditions (Cortesogno et al., 2000), amphiboles developed in different textural sites during the amphibolite to greenschist facies alteration of an olivine gabbro and an Fe-Ti oxide gabbro were analysed for REE, HFSE, LILE, LLE (Li, Be, B) and volatile elements (H, F, Cl) using SIMS.

Brown, amphibolite facies, Mg-hornblendes grading to actinolitic hornblendes (Ti 16795-8645 ppm), which had replaced pyroxenes or filled veins, were analysed. The normalised C1 patterns of the pseudomorphic grains were, on the whole, comparable to those of the higher-temperature titanian amphiboles (Cortesogno et al., 2000), whereas the hornblendes filling the veins showed abundances of normalised Nb, La, Ce, Nd, Sm, Gd, Dy, Y, Er, Yb about 10 times higher with moderately increased Eu. On the contrary, Sr, Zr, Ti, Cr were lower. The REE and trace elements were largely controlled by heritage from clinopyroxene, water–amphibole partitioning and water–rock interactions.

Green hornblendes (Ti 3492-207 ppm) that had filled the veins within the amphibolite facies, at lower temperatures, under the brittle regime, had C1 normalised patterns parallel to those of the brown hornblendes filling the fractures; the element contents being controlled by microsite equilibria. On the whole, the late actinolite filling of the fractures had low trace and RE element contents, and a positive Eu anomaly; the trace and REE element level decreased in the pseudomorphic grains. The tremolite pseudomorphic on olivine had a C1 normalised pattern parallel to, but with lower values than, the vein-filling hornblendes, except for very low Nb. The pattern was also comparable to the vein-filling actinolites, except for higher Dy, Y, Er, Yb and a negative Eu anomaly.

On the whole the H_2O content of the amphiboles decreased and F increased with the metamorphic temperatures, whereas Cl increased in the greenschist facies actinolites.

INTRODUCTION

The interaction between fluids and the oceanic lithosphere has recently been studied using many disciplines and techniques (Alt, 1995, and references therein; Fletcher et al., 1997; Staudigel et al., 1998; Bach and Irber, 1998; ODP Legs 168-169 Shipboard Scientific Party), with significant improvements in the resolution of the investigations and in the refinement of the derived models.

The present study is focused on the behaviour of rare earth and trace elements in the metamorphic amphiboles that developed in the oceanic gabbros from the 117.38 metres cored at ODP Sites 921-924 in the Mid-Atlantic Ridge, between 23°N and the Kane fracture (Leg 153 Shipboard Scientific Party, 1995a and quoted references; ODP Proceedings Scientific Results, 1997; Gaggero and Cortesogno, 1997).

The parent rocks are high to low Mg# troctolites, olivine gabbros, gabbros, and Fe-Ti oxide gabbros respectively (Casey; Cannat et al.; Kempton and Hunter, 1997; Ross and Elthon, 1997; Barling et al., in Karson et al., 1997), which preserve magmatic features and weak to pervasive seafloor metamorphic alteration in localised rock domains.

The present investigation follows and integrates a microtextural and mineral chemistry study (Gaggero and Cortesogno, 1997), and a SIMS study of the igneous and high temperature metamorphic phases (Cortesogno et al., 2000). These studies show the evolution of retrograde metamorphic re-equilibration from very high to low temperature conditions, and from almost closed, rock-dominated systems, towards seawater-dominated systems during the tectonic uplift. During the high-temperature, ductile regime, the recrystallization of the anhydrous assemblages showed an essentially conservative behaviour with regard to the trace and RE elements, but incipient mobilisation, with an exotic supply of elements associated with element-partitioning in the amphiboles from the assemblages, developed through the transitional and brittle regimes (as defined in Cortesogno et al., 2000).

The switch from a ductile to a transitional regime in the seafloor environment was marked by the development of brown amphibole and plagioclase filling and suturing microcracks and fractures. At the regional scale this represents the transition from lateral displacement of the limbs of a slow-spreading ridge to their tectonic uplift coupled with lateral displacement (Cannat et al., 1995; Gillis et al., 1993). Finally, the brittle regime was characterised by greenschist to subgreenschist assemblages in several fracture sets, and represents the shallow-level alteration of the gabbro before its unroofing to the seafloor.

A model of the fluid circulation in the gabbro pile has to consider the penetration of fluids that originated in seawater and were progressively heated with depth and their possible interaction with fluid exsolved from evolved melts. The low-grade alteration induced the release of elements from the shallower rocks, which became concentrated and precip-

itated in the deeper high-T levels. The whole process of recrystallization and chemical mobilisation was the result of a complex pattern evolving over time and in space.

In the MARK gabbros, fractures and veins related to the younging and cooling of the oceanic crust were the apparent paths for the seawater-derived fluids. The veins show several fluid-rock interaction textural patterns such as syntaxial, antitaxial and composite veins. For this reason, particular attention was paid to the transepts from the wall to the core of the veins.

This study is addressed to the element partitioning in the amphiboles from the assemblages that developed through the transitional and brittle regimes.

According to Gaggero and Cortesogno (1997) and references therein, the transition from ductile to brittle deformation is evident in: 1) Late cracks generally showing very low or no displacement (< 1 mm) and opening. Cracks are often restricted to porphyroclasts, evidenced in a more plastic behavior of the matrix; elsewhere, cracks cut the metamorphic banding. 2) Local appearance of fine (maximum size a few mm) cataclastic bands parallel or at a low angle to ductile shear zones. Minerals are affected by grain-size reduction and display irregular grain boundaries; the recrystallization extent is generally low. Brittle textures develop as: 1: Fractures, veins and microcracks filled by secondary phases. Fracture distribution is often irregular and does not exhibit an obvious association with ductile fabrics. Fracturing develops as roughly parallel sets; more rarely, fractures develop an irregular network. 2: Broken and fractured fragments in an extremely fine-grained cataclastic matrix (centimeter to decimeter thick). The alteration of mineral phases is generally extensive.

METAMORPHIC HISTORY OF THE MARK GABBROS

Plutonic rocks in the MARK area are troctolites, olivine gabbros, gabbros, subordinate oxide-gabbros and oxide-diorites (Fe-Ti oxides > 2% in volume); diorites and plagiogranites are restricted to dikelets and veins (Shipboard Scientific Party, 1995).

The igneous petrography of the MARK gabbros is presented in Shipboard Scientific Party (1995), Casey (1997), Cannat et al. (1997), Ross and Elthon (1997), Kempton and Hunter, (1997), Barling et al. (1997). Three main metamorphic regimes were distinguished in the metamorphic evolution of the MARK gabbros by Gaggero and Cortesogno (1997) and Cortesogno et al. (2000).

i) A ductile regime characterised by high-grade, anhydrous to hydrous metamorphic recrystallization (T = 750-1000°C and P ≈ 0.3 GPa) and ductile fabrics.

ii) A transitional regime characterised by medium-T amphibolite facies assemblages (600 <T< 700°C, P ª 0.2 GPa), associated with semi-brittle (e.g. bending and sliding of cleavage or twinning, grain boundary dislocation) to brittle microfabrics.

iii) A brittle regime characterised by low-temperature amphibolite to subgreenschist facies assemblages developed at decreasing temperatures in the estimated range of 600-250°C and P < 0.2 GPa. The recrystallization was controlled by rock-fluid interaction within or at the wall of the fractures.

During the ductile regime, reactions were mostly triggered by deformations, and characterised by grain reduction in the igneous phases and the growth of metamorphic phases during syn-to post-magmatic recrystallization in granoblastic aggregates. Fluid diffusion along shear bands controlled the development of red titanian amphibole (up to 6-7% in volume; Cortesogno et al., 2000).

The foliation that developed in the ductile regime intersected the visco-plastic igneous layering at low angles, and was then cut at high angles by the deformations of the transitional regime, thus suggesting a sharp change in tectonic environment. The transitional and brittle textures generally lie parallel and in some cases the transitional ones were reactivated during the brittle regime.

During the transitional and brittle regimes, the fluid diffusion was the major factor controlling the metamorphic reactions. Fluid diffusion mainly occurred along a mesoscopic - microscopic network of tectonically induced discontinuities, whereas inter- and intra-granular diffusion in undeformed rock domains, revealed by the development of hydrous phases, was generally limited to the centimetre scale.

The incomplete re-equilibration resulted in mineral zoning and in the conservation of compositional heterogeneity, also at a millimetre scale, so that the element distribution can largely depend on different diffusion rates.

ANALYTICAL STRATEGY AND METHODS

Amphibole was the most important phase in the partitioning of RE and trace elements during the transitional and brittle regime. Owing to its complicated and flexible structure, the amphibole crystal-chemistry was extremely sensible to the variation in the intensive parameters of the system. As a consequence, its composition (e.g., the tetrahedral Al and octahedral Ti contents) is frequently used to infer quantitative information on the conditions of crystallization (Liou et al., 1974; Ernst and Liu, 1998, Cortesogno et al., 2000). On the other hand, compositional heterogeneity and zoning preserve the topology of the microtextural domains. In order to reconstruct the metamorphic evolution, two gabbro samples (olivine gabbro 153 921E 3R-1 99-103 and Fe-Ti oxide gabbro 153 921B 3R-1 33-36) were selected as representative of the compositional range of the gabbro suite (see Appendix). The amphiboles that developed in the most representative microtextural domains under different metamorphic conditions were analysed for REE, HFSE, LILE, LLE (Li, Be, B) and volatile elements (H, F, Cl) using a Cameca IMS 4f ion-probe installed at the CNR-C.S. Cristallochimica e Cristallografia of Pavia. The analytical details are reported in Cortesogno et al. (2000, and references therein). A scheme of the analysed phases is reported in Table 1.

Selected whole-rock major and trace element data, amphibole major element data and related analytical details (see Gaggero and Cortesogno, 1997; Cortesogno et al. 2000, for a comprehensive dataset) are reported in Table 2.

MINERAL CHEMISTRY, RARE EARTH AND TRACE ELEMENTS OF AMPHIBOLES

Brown hornblende

The brown hornblendes, which characterised the mineral assemblages during the transitional regime, were Mg-hornblende, sometimes grading to actinolitic hornblendes (Leake et al. 1997). Tschermakitic hornblende compositions also occurred in the oxide-gabbro. The Ti content was in the

Table 1 - Main characteristics of analysed samples and minerals.

Sample	Lithology	Bulk rock composition		Analysed minerals				
				Amphiboles				
		Mg#	TiO_2 wt%	Brown Hbl	Green Hbl	Act	Trm	Titanite
153 921E 3R-1 99-103	Ol-gabbro	69.78	0.47	4	6	2	3	1
153 921B 3R-1 33-36	Fe-Ti Oxide-gabbro	34.21	5.51	4	2			

range 8646-16793 ppm (Table 3; Fig. 1A and B). The Na/(Na+Ca) vs. Al/(Al+Si) ratios (Gaggero and Cortesogno, 1997) showed a positive correlation for increasing pargasite substitution with metamorphic temperatures.

Three hornblende grains in the olivine-gabbro were analysed: a) and a') pseudomorphics on igneous clinopyroxenes affected by folding and sliding of cleavages; b) suturing a microfracture within a clinopyroxene grain (Figs. 1A and 2).

There was a relative homogeneity for the major element composition (Table 2c). C1-normalised trace element patterns showed a moderate LREE depletion (La_N/Yb_N = 0.18-0.20; $HREE_N$ = 40-50), a negative Eu and Sr anomaly, but a positive Zr and Nb anomaly (Fig. 1A). Compared to the igneous and granulitic clinopyroxenes from the gabbros (Cortesogno et al., 2000), the a) and a') amphiboles had a larger proportion of highly-to-moderately incompatible trace elements (mostly LREE and HFSE, namely Ti, Zr and Nb) (Fig. 1A), whereas the Sc and Cr (compatible with both clinopyroxene and amphibole) were similar. The comparison with the high temperature titanian amphibole from the same sample (Cortesogno et al., 2000) pointed to a strong compositional similarity with the amphiboles from a high-strain domain. The main exception was the systematic negative Eu anomaly in the a) and a') amphiboles, which also had a slightly lower Ti, Nb, Sr, La and Ce content. Very similar compositions have also been observed in late-magmatic titanian pargasites in MOR-type gabbroic rocks from the Northern Apennines (Tribuzio et al., 1999; Tribuzio et al., 2000). Moreover, the a) and a') amphiboles showed a higher H_2O content (≈1.6 wt%) than the high-T amphiboles from the same samples, but similar F, Cl (Cl/F ratio in the range 0.02-0.03), Li and Be (mean 0.18 and 0.33 ppm, respectively); B was sometimes higher (up to 1.2 ppm).

Hornblende b) had a REE content about 10 times higher than a) and a') (La_N/Yb_N = 0.23; $HREE_N$ ≈ 700), with the exception of Eu, which was only moderately increased, so that there was a large negative anomaly in the normalised patterns (Fig. 1A). A large negative anomaly was also shown by Sr, Zr and Ti, which were lower than in amphiboles a) and a') (Sr was relatively depleted to magmatic clinopyroxene). Nb was greater than in the a) and a') amphiboles, but Nb_N/La_N was 0.5. On the other hand, the V and Cr contents slightly decreased, whereas the Sc and Ba contents were relatively homogeneous in the brown amphiboles, and the Ba significantly greater than the Ba content in the clinopyroxene. Close similarities were found by Tribuzio et al. (2000) in hornblendes from highly evolved ophiolitic diorites from the Northern Apennines. Finally, the H_2O, Cl and Be contents were significantly higher than in a) and a'), whereas F was lower (Cl/F = 0.16). Li and B were relatively low (0.14 and 0.51 ppm).

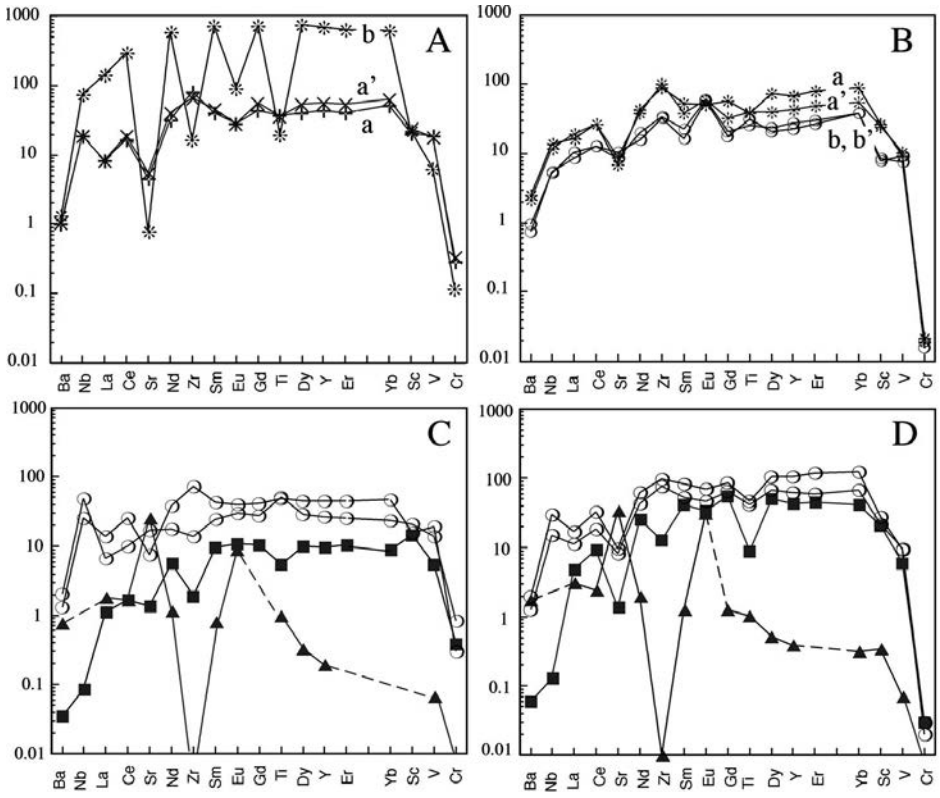

Fig. 1 - Incompatibility spidergrams for the brown hornblendes of the transitional regime. Compositions are normalised to C_1 chondrite (Anders and Ebihara, 1982). A- *Sample 153 921E 3R-1 99-103*. :, pattern a: brown hornblende replacing igneous clinopyroxene at the wall of the vein, spot a) in Fig. 2 ; 5, pattern a': brown hornblende replacing or epitactically overgrowing clinopyroxene, spot a') in Fig. 2; j, pattern b: brown hornblende filling fracture, spot b) in Fig. 2. B- *Sample 153 921B 3R-1 33-36*. :, patterns a and a': brown hornblendes replacing clinopyroxene along microcracks and cleavages; 5, patterns b and b': brown hornblendes replacing and overgrowing clinopyroxene at the clinopyroxene/plagioclase boundary. For comparison m: titanian hornblende and o: igneous clinopyroxene (after Cortesogno et al., 2000). C- patterns of n: igneous clinopyroxene; s: igneous plagioclase; m: high temperature metamorphic titanian amphibole in olivine gabbros (after Cortesogno et al., 2000). D- patterns of n igneous clinopyroxene; s igneous plagioclase; m: high temperature metamorphic titanian amphibole in Fe-Ti oxide gabbro (after Cortesogno et al., 2000).

Table 2 - a- Representative whole–rock composition of ODP Leg 153 gabbros (after Gaggero and Gazzotti, 1996); b- Bulk rock RE element contents of representative gabbroic rocks. Bold: samples selected for SIMS analytical runs (after Cortesogno et al., 2000); c- representative EMP analyses of silicate minerals corresponding to SIMS spots referred both to Cortesogno et al. (2000) and to the present study; d- Rare earth and trace element contents of igneous and high temperature clinopyroxenes (after Cortesogno et al., 2000); e- Rare earth and trace element contents of high temperature titanian amphiboles (after Cortesogno et al., 2000).

Hole	921B	921D	922A	922B	922B	923A	923A	923A	923A	923A	923A
Sample ID	921B 3R 01 46- 52	921D 3R 01 69- 75	922A 2R 05 90- 95	922B 4R 01 48- 52	922B 4R 02 24- 30	923A 9R 01 16- 19	923A 10R 03 113-120	923A 13R 01 129-136	923A 13R 02 27- 36	923A 14R 02 24- 28	923A 15R 02 61- 67
Lithology	Fe-Ti oxide gabbro	Ilm-gabbro w/Pl-granite vein	Ol-gabbro	Troctolite	Troctolite	Magmatic vein	Ol(-Cpx) gabbro	Flaser gabbro	Gabbro	Ol-gabbro w/GHbl vein	Fe-Ti oxide gabbro W/ vein
Oxide wt%											
SiO_2	44.84	53.57	43.02	46.99	44.83	55.88	50.34	49.73	49.98	48.03	47.9
TiO_2	5.51	0.41	1.57	0.16	0.38	1.13	0.29	0.56	0.39	0.26	0.39
Al_2O_3	12.84	14.99	16.7	16.31	17.56	16.24	17.45	18.13	16.85	20.72	19.94
Fe_2O_3	16.67	7.2	10.68	6.00	5.7	7.28	6.31	7.33	7.00	4.8	5.15
MnO	0.28	0.13	0.14	0.08	0.07	0.1	0.12	0.13	0.14	0.08	0.1
MgO	7.8	10.14	13.93	21.00	18.98	4.71	11.3	10.51	11.19	12.09	11.34
CaO	9.19	9.57	9.49	7.44	7.61	6.39	11.42	10.89	11.84	10.73	11.82
Na_2O	2.69	3.02	1.63	0.85	0.96	6.34	2.31	2.49	2.24	1.84	1.85
K_2O	0.08	0.06	0.05	0.02	0.02	0.08	0.03	0.03	0.03	0.04	0.04
P_2O_5	0.05	0.01	1.2	0.03	0.01	1.23	0.00	0.02	0.01	0.01	0.04
LOI	0.01	0.91	1.59	1.12	3.87	0.62	0.43	0.17	0.34	1.4	1.43
Trace ppm											
Ba	31	19	18	16	19	20	21	17	21	17	18
Ce	15	27	23	11	6	100	8	11	5	7	12
Co	128	71	74	40	49	55	70	54	56	42	39
Cr	89	59	164	197	81	15	239	550	1043	291	718
Cu	108	39	66	29	7	33	81	67	73	45	49
La	<2	7	2	2	<2	26	<2	<2	<2	<2	<2
Nb	8	<3	<3	<3	<3	8	<3	<3	<3	<3	<3
Nd	9	15	22	<2	<2	80	<2	3	<2	<2	<2
Ni	63	84	348	627	624	30	125	221	159	286	213
Pb	4	5	5	<2	3	7	5	4	5	5	2
Rb	<4	<4	<4	<4	<4	<4	<4	<4	<4	<4	<4
S	1469	507	1510	21	37	2351	961	787	950	622	731
Sc	54	41	17	6	<5	28	37	35	44	15	22
Sr	113	123	126	111	101	170	138	133	118	136	139
Th	<2	3	<2	<2	<2	2	2	<2	<2	2	<2
U	<2	4	<2	<2	2	<2	<2	<2	<2	3	3
Ga	22	16	17	10	10	24	11	14	12	11	13
Y	41	47	47	8	3	148	9	12	10	6	11
Zn	161	47	103	44	28	33	40	49	45	33	36
Zr	144	154	52	37	25	3070	16	30	24	22	36

Table 2a

		REE (ppm)									
Sample	Lithology	La	Ce	Nd	Sm	Eu	Gd	Dy	Er	Yb	Lu
153 921B 3R01 33-36	**Oxide gabbro**	**1.98**	**6.86**	**8.59**	**3.65**	**1.95**	**5.58**	**7.02**	**4.34**	**4.29**	**0.73**
153 921E 3R-1 99-103	**Ol-gabbro**	**1.03**	**3.35**	**2.71**	**0.66**	**0.4**	**1.05**	**1.11**	**0.69**	**0.75**	**0.12**
153 921D 3R1 69-75	Ilmenite-bearing gabbro (with plagiogranite vein)	6.52	18.3	14.75	4.64	1.28	6.11	7.55	4.83	5.01	0.75
153 921D 5R1 31-35	Gabbro	0.4	1.35	2.01	0.85	0.53	1.46	1.82	1.08	1.05	0.19
153 922A 2R05 90-95	Ol (Cpx. Opx)-gabbro	5.1	19.2	20.5	6.88	1.93	9.14	8.46	4.47	3.36	0.47
153 923A 2R02 74-82	**Gneissic metagabbro**	**0.76**	**3,00**	**2.92**	**0.89**	**0.67**	**1.34**	**1.49**	**0.87**	**0.86**	**0.15**
153 923A 6R02 13-18	Ol-gabbro	0.44	1.36	2.06	0.8	0.56	1.44	1.76	1.04	1.01	0.17
153 923A 9R01 16-19	Ol (Cpx)-gabbro	0.66	2.15	3.41	1.38	0.63	2.22	2.72	1.57	1.56	0.25
153 923A10R01 18-23	**Gabbro (Cpx > 50%)**	**0.35**	**1.22**	**1.64**	**0.68**	**0.52**	**1.21**	**1.52**	**0.9**	**0.83**	**0.16**
153 923A 10R02 19-25	Ol-gabbro	0.31	1.25	1.72	0.74	0.51	1.3	1.58	0.95	0.87	0.19
153 923A 13R01 39-47	Ol-gabbro	0.44	1.07	0.99	0.23	0.33	0.39	0.41	0.21	0.24	0.09
153 923A 13R02 27-36	Gneissic metagabbro	0.51	1.82	2.36	0.94	0.58	1.58	1.95	1.17	1.1	0.2
153 923A 15R02 61-67	Oxide (olivine) gabbro	1.09	3.55	3.62	1.23	0.54	1.79	2,00	1.17	1.15	0.2
153 924B 3R01 4-7	**Ol-gabbro**	**0.22**	**0.75**	**1.25**	**0.51**	**0.37**	**0.97**	**1.3**	**0.8**	**0.72**	**0.16**
153 924B 4W01 50-56	**Ol-gabbro**	**0.54**	**1.56**	**1.59**	**0.61**	**0.45**	**1.13**	**1.36**	**0.82**	**0.79**	**0.17**

Table 2b

Sample ID	**153 921E3R-1 99-103**										
Lithology	**Ol-gabbro**										
Occurrence of mineral phase	Titanian amphibole	Titanian amphibole	Brown Hbl	Brown Hbl	Brown Hbl coex Plg	Act-Hbl	Act-Hbl	Trm	Act	Act	Act
Oxide wt%											
SiO_2	45.27	47.00	49.91	47.15	49.96	47.17	52.9	56.5	52.39	52.84	52.45
TiO_2	3.91	0.18	0.14	1.50	0.25	0.58	0.25	0.02	0.31	0.14	0.44
Cr_2O_3	0.23	0.13	0.00	0.13	0.00	0.08	0.25	0.11	0.14	0.12	1.14
Al_2O_3	10.63	8.38	4.99	8.25	3.90	10.83	1.15	1.09	3.48	1.75	3.87
Fe_2O_3	5.26	5.92	9.78	8.08	12.12	11.38	10.2	4.22	9.04	5.43	3.79
FeO	5.7	11.09	11.99	5.12	8.82	0.00	7.91	4.06	8.24	9.44	8.29
MnO	0.16	0.30	0.24	0.21	0.29	0.19	0.39	0.15	0.28	0.24	0.28
MgO	15.27	12.25	11.03	14.49	12.11	17.05	14.33	19.86	13.82	14.72	15.7
CaO	11.34	12.11	11.1	10.85	10.62	11.11	11.16	12.71	11.04	11.68	12.24
Na_2O	2.41	1.38	0.56	1.62	0.39	2.06	0.00	0.00	0.23	0.00	0.3
K_2O	0.24	0.11	0.16	0.21	0.17	0.26	0.08	0.07	0.16	0.08	0.27
Sum	100.42	98.85	99.90	97.61	98.63	100.71	98.62	98.79	99.13	96.44	98.77
Cations											
Si	6.359	6.838	7.215	6.752	7.254	6.484	7.588	7.798	7.453	7.699	7.438
Ti	0.413	0.020	0.152	0.161	0.027	0.060	0.027	0.002	0.033	0.015	0.047
Cr	0.026	0.015	0.000	0.015	0.000	0.009	0.028	0.012	0.016	0.014	0.128
Al	1.760	1.436	0.850	1.392	0.667	1.755	0.194	0.177	0.584	0.301	0.647
Fe^3	0.556	0.648	1.064	0.948	1.324	1.177	1.100	0.439	0.968	0.595	0.405
Fe^2	0.669	1.349	1.449	0.613	1.070	0.000	0.949	0.469	0.981	1.149	0.984
Mn	0.019	0.037	0.029	0.026	0.036	0.022	0.047	0.017	0.034	0.030	0.034
Mg	3.197	1.656	2.376	3.092	2.621	3.493	3.064	4.085	2.930	3.196	3.318
Ca	1.707	1.877	1.719	1.664	1.652	1.636	1.715	1.879	1.682	1.823	1.859
Na	0.656	0.389	0.157	0.450	0.110	0.549	0.000	0.000	0.063	0.000	0.083
K	0.043	0.020	0.029	0.038	0.032	0.046	0.015	0.012	0.029	0.015	0.049
Sum	15.405	14.285	15.04	15.151	14.793	15.231	14.727	14.89	14.773	14.837	14.992

Sample ID	**153 921B3R-1 33-36**									
Lithology	**Fe-Ti oxide gabbro**									
Occurrence of mineral phase	Igneous Plag	Secondary Plg	Igneous Cpx	Secondary Cpx	Red titanian amphibole	Red titanian amphibole	Titanian amphibole	Brown hbl	Green Act-Hbl	Green Act - Hbl in vein
Oxide wt%										
SiO_2	57.21	56.33	51.61	52.07	43.37	43.37	47.3	47	51.59	51.59
TiO_2	0.07	0.00	0.90	0.36	3.62	3.09	1.50	1.50	0.19	0.24
Cr_2O_3	0.16	0.12	0.30	0.23	0.20	0.18	0.13	0.13	0.07	0.15
Al_2O_3	26.49	26.28	2.09	1.60	11.54	11.37	8.25	8.25	4.24	4.09
Fe_2O_3	0.00	0.00	0.00	0.00	6.56	7.14	0.54	8.89	7.77	7.9
FeO	0.36	0.36	10.36	11.67	6.38	9.34	5.35	5.03	8.82	10.19
MnO	0.06	0.04	0.46	0.36	0.29	0.29	0.21	0.21	0.21	0.34
MgO	0.00	0.00	13.58	12.98	13.37	11.62	14.49	14.49	13.64	12.61
CaO	9.55	9.52	20.79	20.4	11.61	10.94	10.85	10.85	11.45	11.31
Na_2O	5.76	5.86	0.00	0.00	1.42	2.13	1.62	1.62	0.17	0.06
K_2O	0.13	0.13	0.05	0.08	0.32	0.44	0.21	0.21	0.02	0.06
Sum	99.79	98.64	100.14	99.75	98.68	99.91	90.45	98.18	98.17	98.54
Cations										
Si	2.588	2.573	1.936	1.969	6.244	6.265	6.780	6.741	7.409	7.431
Ti	0.002	0.000	0.025	0.010	0.392	0.336	0.161	0.168	0.021	0.026
Cr	0.006	0.004	0.009	0.007	0.023	0.021	0.015	0.018	0.008	0.017
Al	1.412	1.415	0.092	0.071	1.957	1.936	1.386	1.394	0.717	0.694
Fe^3	0.000	0.000	0.000	0.000	0.711	0.776	0.916	0.960	0.840	0.856
Fe^2	0.014	0.014	0.325	0.369	0.768	1.128	0.638	0.604	1.059	1.227
Mn	0.002	0.002	0.014	0.012	0.035	0.035	0.025	0.025	0.025	0.041
Mg	0.000	0.000	0.759	0.732	2.868	2.502	3.078	3.097	2.919	2.707
Ca	0.463	0.466	0.836	0.827	1.790	1.693	1.657	1.667	1.761	1.745
Na	0.519	0.519	0.000	0.000	0.396	0.587	0.448	0.451	0.047	0.016
K	0.007	0.008	0.002	0.004	0.059	0.081	0.038	0.038	0.004	0.011
Sum	5.013	5.001	3.998	4.001	15.243	15.36	15.142	15.163	14.81	14.771

Table 2c

In the oxide-gabbro, four hornblendes were analysed (Table 3, Fig. 1B; Fig. 5): a) and a') that had developed within igneous clinopyroxene grains affected by internal sliding and strain-induced optical anomalies; b) and b') that had overgrown igneous clinopyroxenes and was in equilibrium with plagioclase (An_{35-40}). The C1-normalised pattern of amphibole a) was characterised by a slight LREE depletion (La_N/Yb_N = 0.30; Yb = 80), a positive Zr anomaly, a negative Ti and Sr anomaly, no Eu anomaly and Nb_N/La_N close to 1. These features (Fig. 1B) were comparable with those of both the red titanian amphibole (ductile regime) from the same sample (Cortesogno et al., 2000) and the brown hornblendes a) and a') replacing the clinopyroxene in the olivine gabbro (Fig. 1A). Amphibole a') in the oxide gabbro had a similar LREE, Ba, Zr, Sc, V and Ti content, a slightly higher Sr and Eu content, but a significantly lower Y, and M-HREE. As a consequence a positive Eu anomaly appeared, whereas $LREE_N/MREE_N$ increased and the negative Sr

Sample	924B3R-1 4-7	924B3R-1 4-7	924B3R-1 4-7	923A10R-1 18-23	923A10R-1 18-23	923A2R-2 74-82	923A2R-2 74-82	923A2R-2 74-82	921B3R-1 33-36	921B3R-1 33-36
Lithology	**Ol-gabbro**	**Ol-gabbro**	**Ol-gabbro**	**Gabbro (Cpx > 50%)**	**Gabbro (Cpx > 50%)**	**Granulite**	**Granulite**	**Granulite**	**Fe-Ti oxide gabbro**	**Fe-Ti oxide gabbro**
Occurrence of mineral phase	Igneous cpx	Igneous cpx	Metamorphic cpx	Igneous cpx	Metamorphic cpx	Igneous cpx	Metamorphic cpx	Metamorphic cpx	Igneous cpx	Metamorphic cpx
TiO_2 in the rock	0.23	0.23	0.23	0.29	0.29	0.27	0.27	0.27	5.51	5.51
Elements (ppm)										
K										
Sc	108.91	104.97	93.93	101.53	115.98	106.71	124.85	127.87	120.77	140.17
Ti	3569.87	3237.33	2755.38	2749.42	4300.73	3755.68	4510.31	3037.69	3824.58	2347.52
V	420.49	393.81	352.22	355.36	465.75	530.42	534.44	486.92	328.19	194.41
Cr	1711.99	1613.10	1480.71	1062.01	972.59	533.54	243.50	265.40	80.72	75.71
Rb							4,30			
Sr	9.15	9.01	7.78	9.58	9.72	8.36	10.11	8.39	10.75	9.45
Y	21.61	21.04	18.35	19.25	31.50	22.45	31.39	26.90	67.34	122.73
Zr	14.47	13.03	11.59	10.85	32.93	13.24	21.71	16.68	50.52	90.93
Nb	0.06	0.08	0.05	0.03	0.04	0.01	0.02	0.02	0.03	0.06
Cs										
Ba	0.05	0.14	0.14	0.04	0.19	0.03	0.32	0.04	0.15	0.08
La	0.23	0.24	0.17	0.27	0.42	0.29	0.36	0.41	1.12	2.09
Ce	1.59	1.28	1.32	1.42	2.45	1.50	2.31	2.07	5.78	12.38
Nd	3.39	3.28	2.82	2.94	5.27	2.73	4.90	4.12	11.60	24.83
Sm	1.84	1.75	1.59	1.67	2.69	1.58	2.49	2.09	6.12	12.02
Eu	0.70	0.53	0.48	0.61	1.00	0.68	1.00	0.81	1.92	1.92
Gd	2.63	2.39	2.29	2.86	4.65	2.87	4.87	4.04	10.93	18.73
Dy	3.66	3.51	3.13	3.31	5.71	3.91	5.91	5.03	12.41	23.09
Er	2.21	1.94	1.99	1.83	3.40	2.11	2.99	2.73	7.11	12.92
Yb	2.01	1.75	2.04	1.92	2.70	2.30	2.99	2.44	6.47	12.51
La_N/Yb_N	0.08	0.09	0.06	0.09	0.11	0.08	0.08	0.11	0.12	0.18
La_N/Sm_N	0.08	0.09	0.07	0.10	0.10	0.12	0.09	0.12	0.24	0.30
Gd_N/Yb_N	1.06	1.10	0.91	1.20	1.39	1.01	1.31	1.34	0.61	0.64
∑REE	18.25	16.66	15.82	16.82	28.29	17.95	27.82	23.75	63.46	120.49
∑LREE	7.05	6.54	5.90	6.30	10.84	6.09	10.06	8.69	24.62	51.32
∑HREE	10.51	9.59	9.45	9.91	16.46	11.18	16.76	14.25	36.92	67.25

Table 2d

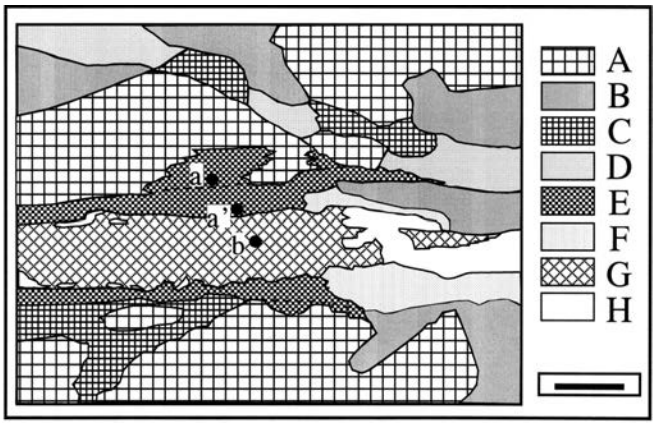

Fig. - 2: *Sample 153 921E 3R-1 99-103, Olivine-gabbro*. Microtextural sketch. Brown hornblende developed along a fracture replacing the wall-rock clinopyroxene and filling the vein. The fracture, which developed under the transitional regime, cuts across granoblastic stripes of the ductile regime. Legend: A- Igneous clinopyroxene. B- Igneous plagioclase (An_{70-75}). C- Granoblastic clinopyroxene + titanian amphibole (Ductile regime). D- Granoblastic plagioclase (An_{70}; Ductile regime). E- Brown hornblende replacing or overgrowing igneous and metamorphic clinopyroxenes ± titanian amphibole F- Secondary plagioclase (An_{47}) overgrowing an optical continuity of the igneous plagioclase. G- Vein-filling brown hornblende. H- Vein-filling plagioclase (An_{47}). Scale bar corresponds to 1 mm. a), a') and b) are the analysed spots.

anomaly decreased. Analogous compositional variations were reported by Tribuzio et al. (2000) in late-magmatic amphiboles affected by metamorphic re-equilibration.

Overall, amphiboles b) and b') had lower trace element levels, with the exception of Eu, Sr, V and Cr, which were from slightly lower to higher than in a'). This determined a further increase in the positive Eu anomaly and a strong attenuation of the negative Sr anomaly.

The comparison with the igneous clinopyroxene highlights the increase in Ba, Nb, La, Sr, Zr and Ti in hornblendes a) and a'). On the contrary, hornblendes b) and b') have lower HREE, Y and Sc.

Unlike the trace elements, the brown hornblendes from the oxide-gabbro do not show a significant and systematic variation in the proportion of volatile and light elements, which are similar to those of the high-T amphiboles from the same sample. Amphibole a) has the maximum Cl content (110 ppm) and Cl/F ratio (0.08), whereas amphibole b) has the maximum B content (1.2 ppm). As a whole, brown hornblendes from oxide gabbro are richer in Be and poorer in Li than those from olivine gabbro (Table 3).

Green hornblende

The green hornblendes that developed under the relatively high temperature conditions of the brittle regime are acti-

Lithology	Ol-gabbro	Ol-gabbro	Gabbro (Cpx > 50%)	Granulite	Fe-Ti oxide gabbro	Fe-Ti oxide gabbro	Fe-Ti oxide gabbro
Occurrence of mineral phase	Red hbl	Red brown hbl	Red hbl	Red hbl	Red hbl granoblastic	Red brown hbl granoblastic	Red brown hbl zoning
TiO_2 in the rock	0.47	0.47	0.29	0.27	5.51	5.51	5.51
Elements (ppm)							
K	915.08	2121.38	1018.39	1057.92	1926.00	1863.87	1698.75
Sc	119.85	89.30	150.58	160.57	147.24	189.20	128.06
Ti	22239.39	20904.12	20529.33	22843.55	19088.58	18477.42	18196.02
V	793.13	1104.86	942.61	1065.91	524.11	493.56	547.71
Cr	2261.24	813.10	1659.93	299.71	83.49	55.84	89.87
Rb	4.64	7.97	6.74	6.87	9.54	9.53	10.89
Sr	131.22	58.65	45.09	54.78	54.97	53.68	63.22
Y	42.16	69.74	68.26	66.25	121.71	123.02	96.56
Zr	53.81	287.44	68.26	48.24	372.08	337.19	300.89
Nb	12.12	6.19	0.90	1.17	5.89	4.96	3.77
Cs			0.04				
Ba	4.84	3.10	2.37	2.48	4.43	4.99	2.97
La	1.60	3.33	1.12	0.90	5.10	3.07	2.71
Ce	6.10	15.91	6.57	5.28	24.62	14.65	11.46
Nd	8.14	17.81	12.64	10.94	32.29	19.60	19.63
Sm	3.61	6.35	6.27	5.59	11.84	8.25	8.04
Eu	1.66	2.21	2.07	2.02	4.50	3.05	2.62
Gd	5.48	8.11	8.86	8.37	15.88	13.05	12.86
Dy	7.01	11.15	11.33	10.72	20.75	20.06	16.86
Er	4.16	7.18	6.79	6.72	13.28	15.10	9.46
Yb	3.75	7.41	5.54	5.98	14.79	17.35	10.76
La_N/Yb_N	0.29	0.30	0.14	0.10	0.23	0.12	9.70
La_N/Sm_N	0.28	0.33	0.11	0.10	0.27	0.12	2.44
Gd_N/Yb_N	1.18	0.88	1.29	1.13	0.87	1.36	3.90
∑REE	41.49	79.45	61.19	56.52	143.03	114.17	94.42
∑LREE	19.45	43.40	26.59	22.70	73.85	45.57	41.84
∑HREE	20.39	33.84	32.52	31.80	64.69	65.56	49.95

Table 2e

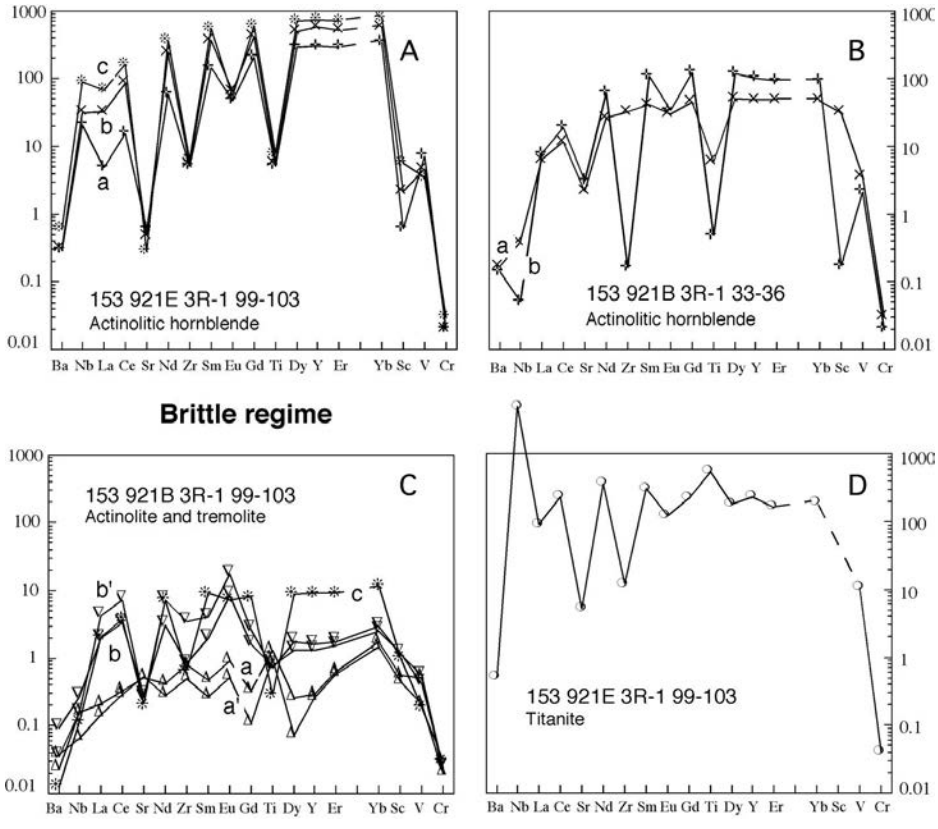

Fig. 3 - Incompatibility spidergrams for the green hornblendes of the brittle regime. Compositions are normalised to C_1 chondrite (Anders and Ebihara, 1982). A- *Sample 153 921E 3R-1 99-103.* Filling-vein actinolitic hornblendes: ;, pattern a- epitaxial growth; 5, S, patterns b- and c- aggregates of prismatic elongated crystals. B- *Sample 153 921B 3R-1 33-36.* 5, pattern a: actinolitic hornblende replacing igneous clinopyroxene and brown hornblende; ;, pattern b- fracture-filling actinolitic hornblende. C- *Sample 153 921E 3R-1 99-103.* D, patterns a- and a'- actinolite filling a vein across igneous clinopyroxene; —, pattern b- actinolite filling a vein across plagioclase; D- *Sample 153 921E 3R-1 99-103.* ;, pattern a: tremolite pseudomorph at olivine rim; S, patterns b- and b'- tremolite pseudomorph at olivine core. E: *Sample 153 921E 3R-1 99-103.* Neoblastic titanite within vein.

Table 3 - Rare earth and trace element contents of brown amphibole. Concentrations are expressed in parts per million (ppm). Rare earth element ratios are chondrite-normalised, with chondrite values from Anders and Ebihara (1982).

Sample	153 921E 3R-1 99-103	153 921E 3R-1 99-103	153 921E 3R-1 99-103	153 921B 3R-1 33-36	153 921B 3R-1 33-36	153 921B 3R-1 33-36	153 921B 3R-1 33-36
Lithology	Olivine gabbro	Olivine gabbro	Olivine gabbro	Fe-Ti oxide gabbro	Fe-Ti oxide gabbro	Fe-Ti oxide gabbro	Fe-Ti oxide gabbro
Textural features	Brown Hbl pseudomorph on Cpx (a in Fig. 1A)	Brown Hbl pseudomorph on Cpx (a' in Fig. 1A)	Brown Hbl filling vein (b in Fig. 1A)	Brown Hbl pseudomorph on Cpx core (a in Fig. 1B)	Brown Hbl pseudomorph on Cpx (a' in Fig. 1B)	Brown Hbl reaction rim on Cpx (b in Fig. 1B)	Brown Hbl reaction rim on Cpx (b' in Fig. 1B)
Analysis n°.	1	2	3	4	5	6	7
Elements (ppm)							
K	1988	1698	1194	2105	2012	1043	937
Sc	120	141	130	153	140	45	49
Ti	16793	15919	8646	16401	17204	13407	11155
V	1081	1037	359	530	599	513	431
Cr	776	890	314	59	51	42	51
Rb	*bdl*	*bdl*	3	4	*bdl*	*bdl*	*bdl*
Sr	36	44	6,2	54	70	80	67
Y	68	89	1102	106	68	35	44
Zr	328	262	67	352	402	129	133
Nb	4.7	4.6	18	3.5	2.9	1.3	1.3
Cs	-	-	-	-	-	-	-
Ba	2.4	2.5	3.1	5.8	5.0	2.2	1.8
La	1.99	2.02	34.0	3.8	4.5	2.42	2.03
Ce	10.5	11.7	187.3	16.1	16.7	7.8	8.0
Nd	14.5	18.5	272.9	19.9	17.7	7.2	9.2
Sm	6.2	7.1	107.9	8.0	5.7	2.44	3.4
Eu	1.57	1.58	5.2	2.88	3.3	3.2	3.4
Gd	8.7	11.0	146.0	11.3	6.5	3.4	4.1
Dy	10.2	13.4	190.9	17.7	9.9	5.0	5.8
Er	6.5	8.8	104.6	12.7	7.7	4.2	4.9
Yb	8.2	10.2	101.0	14.2	8.6	6.0	6.0
La_N/Yb_N	0.16	0.13	0.23	0.18	0.35	0.27	0.23
La_N/Sm_N	0.20	0.18	0.20	0.30	0.50	0.63	0.38
Eu/Eu*	0.65	0.55	0.13	0.93	1.7	3.4	2.8
Ti/Ti*	0.90	0.66	0.03	0.58	1.1	1.6	1.2
Sr/Sr*	0.19	0.19	0.002	0.20	0.27	0.72	0.52
F	1753	2934	1278	1421	2153	1714	1714
Cl	57	57	203	110	38	76	76
Li	0.17	0.21	0.14	0.13	0.079	0.075	0.075
Be	0.33	0.32	3.0	0.69	0.69	0.49	0.49
B	1.2	0.43	0.51	1.0	0.6	1.2	1.2
H_2O (%)	1.60	1.62	1.72	1.49	1.37	1.50	1.50

nolitic hornblende (Leake et al., 1997) with Ti in the range 207-3492 ppm (Table 4; Fig. 4A and B). Brown and green hornblendes locally show intermediate textural features and mineral compositions; in most cases, cracks that developed under the transitional regime were reactivated under the brittle conditions.

Three actinolitic hornblendes in the olivine gabbro were analysed (Fig. 5): a) filling a 1 mm-thick vein together with oligoclase and titanite; b) filling a 0-7 mm-thick vein together with oligoclase; c) suturing an epitaxial overgrowth of a clinopyroxene grain cut by a 0-8 mm vein.

The Ti contents of the amphiboles analysed increased progressively from a) (2232 ppm) to c) (3492 ppm) together with Nb, La, Ce, Nd, Sm, Gd, Dy, Y (up to 1145 ppm), Er, Yb, Sc (up to 34 ppm). A moderate decrease was observed for V (from 411 to 200 ppm), Sr (4.8-2.2 ppm) and Rb (up to 10 ppm), whereas Zr, Eu and Cr were slightly increased. Normalised patterns were LREE-depleted [La_N/Yb_N from 0.01 in a) to 0.08 in c), respectively] and showed marked negative Sr, Zr, Eu and Ti anomalies. Parallelism with the normalised pattern of the brown, fracture-filling, hornblende arises/There is a similarity to the normalised pattern of the brown-fracture-filling hornblende (b in Fig. 1A).

The quantity of the trace elements was also strongly correlated with the variation in Be and B, reaching higher values in the a) amphibole (8.3 and 3.1 ppm, respectively), whereas Li was constantly low (£ 0.33 ppm). Important variations were also displayed by the volatile elements. Cl attained significant values [up to 1574 ppm in amphibole a)] and the Cl/F was always > 1. The H_2O content was high, the oxy-component becoming progressively subordinated as the Ti decreased.

Two actinolitic hornblendes in the oxide-gabbro were analysed (Table 4; Fig. 4B): a) pseudomorphic after igneous clinopyroxene and brown amphibole at the selvedge of a 0-1 mm vein. b) filling the vein together with oligoclase. The pseudomorphic amphibole a) showed REE and Ti contents coincident with those of the igneous clinopyroxene (see Fig. 1D). The Zr content was significantly higher, and Ba, Sr and Nb showed slight increases. In general, amphibole a) had an

intermediate composition between the igneous clinopyroxene and amphiboles from the granulitic or transitional regimes.

The vein-filling amphibole b) was characterised by higher Y and REE but markedly lower Nb, Zr, Ti and Sc contents. In spite of its lower abundance, the normalised patterns were very similar to those of the vein-filling hornblendes from the olivine gabbro, being characterised by La_N/Yb_N=0.08 and large negative Eu, Sr, Zr and Ti anomalies. Amphibole b) also showed high H_2O and Cl contents (1.91 wt% and 2100 ppm, respectively), low Li and Be content and a very low amount of F (66 ppm).

Actinolite and tremolite

Five analyses were performed along a millimetric transept in the olivine gabbro: a) and a') actinolite partially replacing igneous clinopyroxene interstitial between plagioclase and altered olivine; b) and b') actinolites overgrowing the interstitial clinopyroxene, which had developed towards the olivine microdomain; c) tremolite, from the tremolite–chlorite mat, replacing olivine (Table 5; Fig. 4C, D).

Actinolite a) and a') had noticeably lower RE and trace element contents than their ancestor igneous clinopyroxene (Fig. 1C). The normalised values were systematically below 1 time C1, except for Yb. The normalised patterns were characterised by a convex-upward shape in the L-MREE part (La_N/Sm_N = 0.44-0.55), in which a significant positive Eu anomaly occurred, and by a steep positive slope in the HREE (La_N/Yb_N = 0.10-0.12). Sr_N, Zr_N and Ti_N were higher than the adjacent REE, whereas Ba_N and Nb_N were lower than La_N, even if they defined a smooth fractionation trend in the spiderdiagrams. The H_2O content was high (1.98-2.06 wt%), whereas both the F and Cl were very low (hundreds and tens of ppm, respectively). Li, Be and B were nearly constant and in very low quantities (lower than 0.07, 0.41 and 0.28 ppm, respectively). Compared to the b) and b') actinolites, they showed extremely depleted REE (especially L-MREE), whereas they had similar Ba, Nb, Sc and Cr contents.

The normalised patterns of the b) and b') actinolites had an L-MREE-enriched sigmoidal shape (maximum at Ce_N = 3.3-7.4; La_N/Yb_N = 0.81-1.44) and were characterised by an evident positive Eu anomaly. Highly incompatible (Nb, Ba, Sr) and compatible (Sc, Cr) elements and the LREE and LILE were similar to those of tremolite c), but the HREE was lower. H_2O was nearly stoichiometric. The F and Cl contents were low, but positively correlated. The B content was always high (1.14-2.72 ppm), whereas Li was very variable (0.04-2.05 ppm).

The normalised pattern of tremolite c) showed a significant parallelism with that of the vein-filling hornblendes (La_N/Yb_N = 0.18), in spite of normalised contents that were lower by one order of magnitude. The tremolite showed similar Ba, Nb and REE to the igneous clinopyroxene, but largely lower Sr, Zr, Ti, V, Sc and Cr. The H_2O content was the highest of the analysed amphiboles (mean 2.08 wt%). The Cl was relatively high (137-285 ppm), but the Cl/F was <<1 (0.14-0.18). As in the case of the LLE, the Li content was very low (0.02 ppm), whereas B was in the range 2.86-3.4 ppm (Fig. 6).

Trace and rare earth element content of titanite

The titanite developed during the brittle events as: i) a breakdown product of ilmenite, ii) the segregation by replacement of titanian amphibole by actinolitic hornblende and/or actinolite, iii) the fracture-filling phase, together with green hornblende + oligoclase or actinolite + albite.

One euhedral grain (0.3 mm) of titanite in equilibrium with actinolitic hornblende (Table 5, Figs. 3 and 4D) and oligoclase, filling a fracture, was analysed. The REE content was high (∑REE= 540 ppm); the normalised pattern showed very high Nb, high Ce, Nd, Sm, low Sr, Zr and Eu and very low V and Cr.

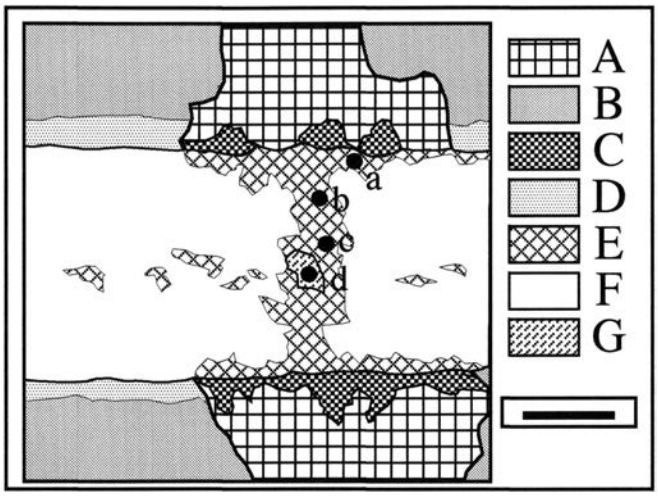

Fig. 4 - *Sample 153 921E 3R-1 99-103, Olivine-gabbro*. Microtextural sketch. Vein-filling actinolitic hornblende and oligoclase. The fracture developed under the brittle regime, reactivating a microcrack (Transitional regime) marked by brown hornblende and plagioclase. Legend: A- Igneous clinopyroxene. B- Igneous plagioclase ($An_{\sim 70}$). C- Brown hornblende. D- Secondary plagioclase ($An_{\sim 47}$). E- Vein-filling actinolitic hornblende. F- Vein-filling oligoclase ($An_{\sim 22}$). G- Titanite. Bar scale corresponds to 0.1 mm. a), b) c) and d) are the analysed spots.

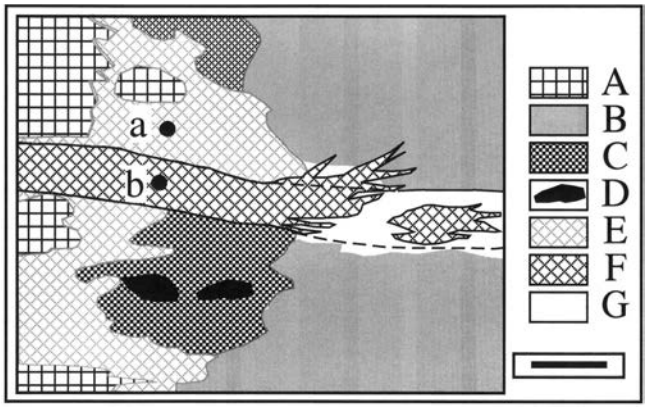

Fig. 5 - *Sample 153 921B 3R-1 33-36, Oxide-gabbro.* Microtextural sketch. Legend: A- Igneous clinopyroxene. B- Igneous plagioclase partially re-equilibrated during the transitional regime. C- Brown hornblende (Transitional regime). D- Ilmenite and magnetite (Transitional regime). E- Actinolitic hornblende replacing clinopyroxene and brown hornblende. F- Vein-filling actinolitic hornblende. G- Vein-filling oligoclase. a- and b- are the analysed spots.

DISCUSSION

Various factors are believed to control the element concentration in amphiboles, of these the following are discussed: 1) crystallographic constraints 2) equilibrium temperatures 3) microtextural site and associated mineral phase

Table 4 - Rare earth and trace element data for green hornblende. Concentrations are expressed in parts per million (ppm). Rare earth element ratios are chondrite-normalised, with chondrite values from Anders and Ebihara (1982).

Sample	153 921E 3R-1 99-103	153 921E 3R-1 99-103	153 921E 3R-1 99-103	153 921E 3R-1 99-103	153 921E 3R-1 99-103	154 921B 3R-1 33-36	155 921B 3R-1 33-36	156 921B 3R-1 33-36
Lithology	Olivine gabbro	Olivine gabbro	Olivine gabbro	Olivine gabbro	Olivine gabbro	Fe-Ti oxide gabbro	Fe-Ti oxide gabbro	Fe-Ti oxide gabbro
Textural features	Act Horn filling vein w/ Ttn (a in Fig. 4A)	Act Horn filling vein w/ oligoclase (b in Fig. 4A)	Act Horn filling vein w/ oligoclase (b in Fig. 4A)	Act Horn filling vein (c in Fig. 4A)	Act Horn filling vein (c in Fig. 4A)	Act Horn pseudomorphic on igneous Cpx (a in Fig. 4B)	Act Horn filling vein w/ oligoclase (b in Fig. 4B)	Act Horn filling vein w/ oligoclase (b in Fig. 4B)
Analysis n°.	1	2	2'	3	3'	4	5	5'
Elements (ppm)								
K	1080	1521	-	2177	-	342	176	-
Sc	4	13	-	34	-	182	<1	-
Ti	2232	2428	2428	3492	3492	2529	207	207
V	411	265	-	200	-	203	121	-
Cr	45	54	-	75	-	80	45	-
Rb	9	10	-	7	-	*bdl*	4	-
Sr	4.8	3.8	-	2.2	-	17	24	-
Y	482	892	892	1145	1145	76	157	157
Zr	20	22	-	25	-	127	0.63	-
Nb	5.1	7.7	-	22	-	0.10	0.01	-
Cs	-	0.08	-	-	-	0.04	-	-
Ba	0.67	0.75	-	1.4	-	0.39	0.33	-
La	1.14	7.59	7,59	15,7	15,72	1,49	1,84	1,84
Ce	9.6	52.7	52.7	101.4	101.4	7.2	11.7	11.7
Nd	27.5	109.0	109.0	172.7	172.7	12.2	28.2	28.2
Sm	21.5	55.5	55.5	82.0	82.0	6.2	16.3	16.3
Eu	2.67	3.6	3.6	3.1	3.1	1.66	1.91	1.91
Gd	42.0	82.4	82.4	119.3	119.3	8.8	24.6	24.6
Dy	70.9	123.4	123.4	175.7	175.7	12.6	29.0	29.0
Er	46.9	83.6	83.6	113.9	113.9	7.9	15.0	15.0
Yb	55.1	91.6	91.6	128.6	128.6	7.6	14.9	14.9
La_N/Yb_N	0.01	0.06	0.06	0.08	0.08	0.13	0.08	0.08
La_N/Sm_N	0.03	0.09	0.09	0.12	0.12	0.15	0.07	0.07
Eu/Eu*	0.27	0.16	0.16	0.10	0.10	0.69	0.29	0.29
Ti/Ti*	0.02	0.01	0.01	0.01	0.01	0.12	0.004	0.004
Sr/Sr*	0.02	0.003	0.003	0.001	0.001	0.11	0.08	0.08
F	612	1019	986	1043	1048		44	66
Cl	716	1305	1327	1574	1270		1287	2162
Li	0.18	0.13	0.14	0.12	0.33		0.19	0.12
Be	1.9	4.8	5.3	8.3	8.0		0.16	0.15
B	0.24	1.4	1.5	2.6	3.1		0.97	0.95
H_2O (%)	1.92	1.93	1.94	1.74	1.80		1.96	1.91

44) water/amphibole partitioning coefficient 5) composition of the fluid phase 6) rock/water ratios.

Of the major elements in the amphiboles, Al, Si and, mostly, Ti correlate with the metamorphic temperatures (Gaggero and Cortesogno, 1997). The RE, trace, light lithophile and volatile elements highlight an increased, positive correlation with factors other than temperature. The composition of the amphiboles is discussed in relation to the microtextural site.

Pseudomorphic amphiboles

At relatively high T, the brown hornblendes replacing clinopyroxene grains (patterns a and a' in Figs. 1A and B; analyses Am #1, 2, 4, 5 in Table 3) have Ti in the range 15919-17204 ppm, a slightly negative or positive Eu anomaly and a positive Zr anomaly (Zr between 262-402 ppm). They show a rough similarity to their ancestor clinopyroxene (Fig. 1C and D), but have higher ∑REE (in particular LREE) and trace elements (mostly Zr and Nb).

The pseudomorphic green hornblende (analysis #4 in Table 4) has a RE and trace element content similar to that of homologous brown hornblendes, except for lower Ti, no Zr anomaly and a weak negative Eu anomaly. In both the brown and green hornblendes the LREE/HREE (0.6-1.3) and MREE/HREE (0.3-0.8) ratios were low (Figs. 1A, B and 2B) and Nb/La varied from > 1 (olivine gabbro) to ≤ 1 (oxide gabbro). On the whole, the comparison with the ancestor pyroxene suggested an important compositional heritage, together with RE and trace element introduction with fluids.

The brown hornblendes that developed through a reaction involving both pyroxene and the surrounding plagioclase and oxides (b an b' in Fig. 1B; analyses Am# 6 and 7 in Table 2) showed significant differences to the pseudomorphic brown hornblendes (lower Ti, Zr, Nb SREE and HFSE, but higher Sr and Eu, $LREE_N/MREE_N$ and $LREE_N/HREE_N$), which were consistent with reactions and element partitioning that mostly involved plagioclase.

The pseudomorphic actinolites had significantly lower REE and trace elements than their ancestor clinopyroxene (patterns a and a' in Fig. 4D; analyses 7-8 in Table 5), mostly for L- and MREE and Dy, with low Y, V, Sc and Cr, suggesting element partitioning in the fluid phase during the greenschist facies metamorphic reactions.

The alteration of olivine to chlorite (at the rim) and tremolite (prevailing at the core) reflected the introduction of Ca, Si, and Al by fluids and their differential mobility (Cortesogno et al., 1975). Due to the negligible contribution of olivine and the negligible role of chlorite, the abundance

Table 5 - Rare earth and trace element data for actinolites, tremolite and titanite. Concentrations are expressed in parts per million (ppm). Rare earth element ratios are chondrite-normalised, with chondrite values from Anders and Ebihara (1982).

Sample	153 921E 3R-1 99-103	153 921E 3R-1 99-103	153 921E 3R-1 99-103	153 921E 3R-1 99-103	153 921E 3R-1 99-103	153 921E 3R-1 99-103	153 921E 3R-1 99-103	153 921E 3R-1 99-103
Lithology	Olivine gabbro	Olivine gabbro	Olivine gabbro	Olivine gabbro	Olivine gabbro	Olivine gabbro	Olivine gabbro	Olivine gabbro
Textural features	Act replacing Cpx (a in Fig. 4C)	pseudomorphic on Cpx (a' in Fig. 4C)	Act overgrowing Cpx/Ol (b in Fig. 4C)	Act overgrowing Cpx/Ol (b in Fig. 4C)	Act overgrowing Cpx/Ol (b' in Fig. 4C)	Trm on Ol (c in Fig. 4C)	Trm on Ol (c in Fig. 4C)	Ttn (Fig. 4D)
Analysis n°.	7	8	9	9'	10	11	11'	12
Elements (ppm)								
K	77	97	270	-	389	151	-	-
Sc	3	3	7	-	7	6	-	<1
Ti	562	424	340	340	316	128	128	237261
V	29	12	24	-	32	11	-	602
Cr	53	54	66	-	64	83	-	94
Rb	3	2	*bdl*	-	*bdl*	*bdl*	-	<1
Sr	4.0	4.1	2.2	-	2.1	1.6	-	41
Y	0.46	0.40	2.1	2.1	2.5	14.6	14.6	365
Zr	3.2	1.9	3.3	-	14	2.6	-	48
Nb	0.04	0.02	0.07	-	0.04	0.03	-	1292
Cs	-	-	-	-	-	-	-	-
Ba	0.06	0.09	0.22	-	0.08	0.03	-	1.2
La	0.05	0.04	0.47	0.47	1.02	0.49	0.49	21.5
Ce	0.20	0.18	2.03	2.03	4.5	2.35	2.35	145.3
Nd	0.19	0.13	1.39	1.39	3.3	3.3	3.3	171.7
Sm	0.07	0.04	0.29	0.29	0.62	1.40	1.40	46.1
Eu	0.05	0.03	0.47	0.47	0.99	0.41	0.41	7.0
Gd	0.07	0.02	0.32	0.32	0.51	1.59	1.59	45.5
Dy	0.06	0.02	0.32	0.32	0.43	2.18	2.18	46.2
Er	0.10	0.09	0.25	0.25	0.28	1.46	1.46	26.4
Yb	0.28	0.24	0.39	0.39	0.48	1.88	1.88	30.0
La_N/Yb_N	0.12	0.10	0.81	0.81	1.4	0.18	0.18	0.48
La_N/Sm_N	0.44	0.55	1.0	1.0	1.0	0.22	0.22	0.29
Eu/Eu*	2.2	2.7	4.7	4.7	5.2	0.84	0.84	0.46
Ti/Ti*	4.3	10.6	0.53	0.53	0.33	0.03	0.03	2.6
Sr/Sr*	1.4	1.9	0.09	0.09	0.04	0.04	0.00	0.02
F	130	153	456	786	950	1587	949	
Cl	20	11	82	109	221	285	137	
Li	0.07	0.05	2.05	0.59	0.04	0.02	0.02	
Be	0.41	0.32	0.30	0.17	0.10	0.40	0.21	
B	0.21	0.28	1.7	1.1	2.7	3.4	2.9	
H_2O (%)	1.98	2.06	1.95	1.96	1.91	2.02	2.14	

of REE (in particular LREE) and trace elements in tremolite supports a supply by entering fluids.

When compared with vein-filling hornblendes, the low REE content in tremolite suggests possibly lower element concentrations in the hydrous fluids at the greenschist facies conditions, but this could also depend on the higher solubility of the REE, due to the stability of chloride complexes, as well as crystallography.

The actinolites that developed at the clinopyroxene-olivine interface (b, b' in Fig. 4D; analyses Am# 9-10 in Table 5) showed intermediate patterns, except for evident positive Eu anomalies and higher Ba, Nb, La, Ce. The positive Eu anomaly in the actinolites was probably controlled by the breakdown of plagioclase to albite, whereas the buffering effect of albite which has $^{solid/L}D > 1$ for Ba and Sr (Blundy and Wood, 1994) may account for their low contents.

Amphiboles filling veins

In the olivine gabbro, the vein-filling brown (b in Fig. 1A; analysis Am# 3 in Table 3) and green (a, b, c in Fig. 4A; analyses Am# 1, 2 and 3 in Table 4) hornblendes are characterised by high REE, Nb, Be, B, and Cl, and a sharp negative Sr, Eu, Ti and Zr anomaly. The apparent parallelism of the patterns suggests the homogeneous composition of the fluids, and little correlation with the metamorphic grade except for Ti.

The compositional zoning of the amphiboles in the veins can be interpreted as due to progressive fluid dilution, possibly induced by precipitation in the solid phase.

At relatively low temperatures (brittle regime) the local precipitation of titanite in the veins of the Ol-gabbro indicates Ti enrichment in the fluid phase, probably as a consequence of ilmenite breakdown and of decreased Ti uptake in the amphibole structure. On the other hand, the element partitioning with titanite can account for the decrease of most RE and trace elements in the co-existing actinolitic hornblende (a in Fig. 4A; analysis Am# 1 in Table 4). Accordingly, the widespread growth of secondary titanite in the oxide-gabbro (Fig. 4E) can account for the relatively low level of RE and trace elements, in particular Nb, in the vein-filling actinolitic hornblende (analysis Am# 5 in Table 5).

Trace and rare earth element behaviour

Important mobilisation by fluids and partitioning in the hornblendes at high temperature conditions are implied mostly for Nb, La, Ce, Nd, Sm, Gd, Dy, Y, Er and Yb. Lower concentrations in the fluids and/or $^{solid/fluid}D$ are suggested by the tremolite composition.

The Sc, V and Cr concentrations remained almost constant during the alteration of igneous clinopyroxene to hornblende, indicating a virtual lack of mobilisation; moreover the relative increase in volume following hydration possibly accounts for small decreases. Low mobilisation rates for Sc and Cr in the fluid phase, and for Zr are also consistent with

the low contents in vein-filling hornblendes. On the other hand, the Zr increase during the alteration of clinopyroxene to hornblende, can probably be attributed to reactions involving interstitial igneous Zr phases, thus implying only short-range mobilisation. The Ti had a similar behaviour, apart from the inferred positive correlation with the metamorphic temperatures (Cortesogno et al., 2000).

The Eu increased during the alteration of the clinopyroxene to brown hornblendes, (Eu_{cpx} = 0.48-0.70 ppm, Eu_{Hbl} = 1.57-1.58 ppm in Ol-gabbro and Eu_{cpx} = 1.92-2.17 ppm, Eu_{Hbl} = 2.88-3.4 ppm in ox-gabbro). In the vein-filling hornblendes, the Eu had relatively high absolute values but negative anomalies in accordance with the plagioclase buffer (Figs. 1A, 4B). In the oxide-gabbro, the pseudomorphic brown hornblendes in contact with plagioclase had a positive Eu anomaly (b and b', Fig. 1B); possibly the buffer of high modal oxides can increase Eu^{2+}/Eu^{3+} with a consequent increase in $Eu^{2+,\ 3+}/REE^{3+}$ in the amphibole. The relatively high concentration of Eu in low-T hydrothermal fluids following the alteration of igneous plagioclase to albite or albite + adularia at lower temperatures (Bach and Irber, 1998; Vanko and Laverne, 1998), can account for the positive (in actinolites) or weak negative (in tremolite) Eu anomalies in greenschist facies amphiboles.

The Sr content is higher in the pseudomorphic brown hornblendes than in the clinopyroxene; in the vein-filling hornblendes as well as in the tremolites and actinolites coexisting with plagioclase or, respectively, albite, the Sr content was significantly lower, possibly due to preferential partitioning in the feldspar. Furthermore, the very low Ba content in the greenschist facies amphiboles could depend on its compatibility with albite (Blundy and Wood, 1994), whereas K (incompatible with albite) had moderately high contents.

Volatile and LLE behaviour

The volatile and LL elements were correlated with the Ti contents (Fig. 6), assumed to be indicative of the metamor-

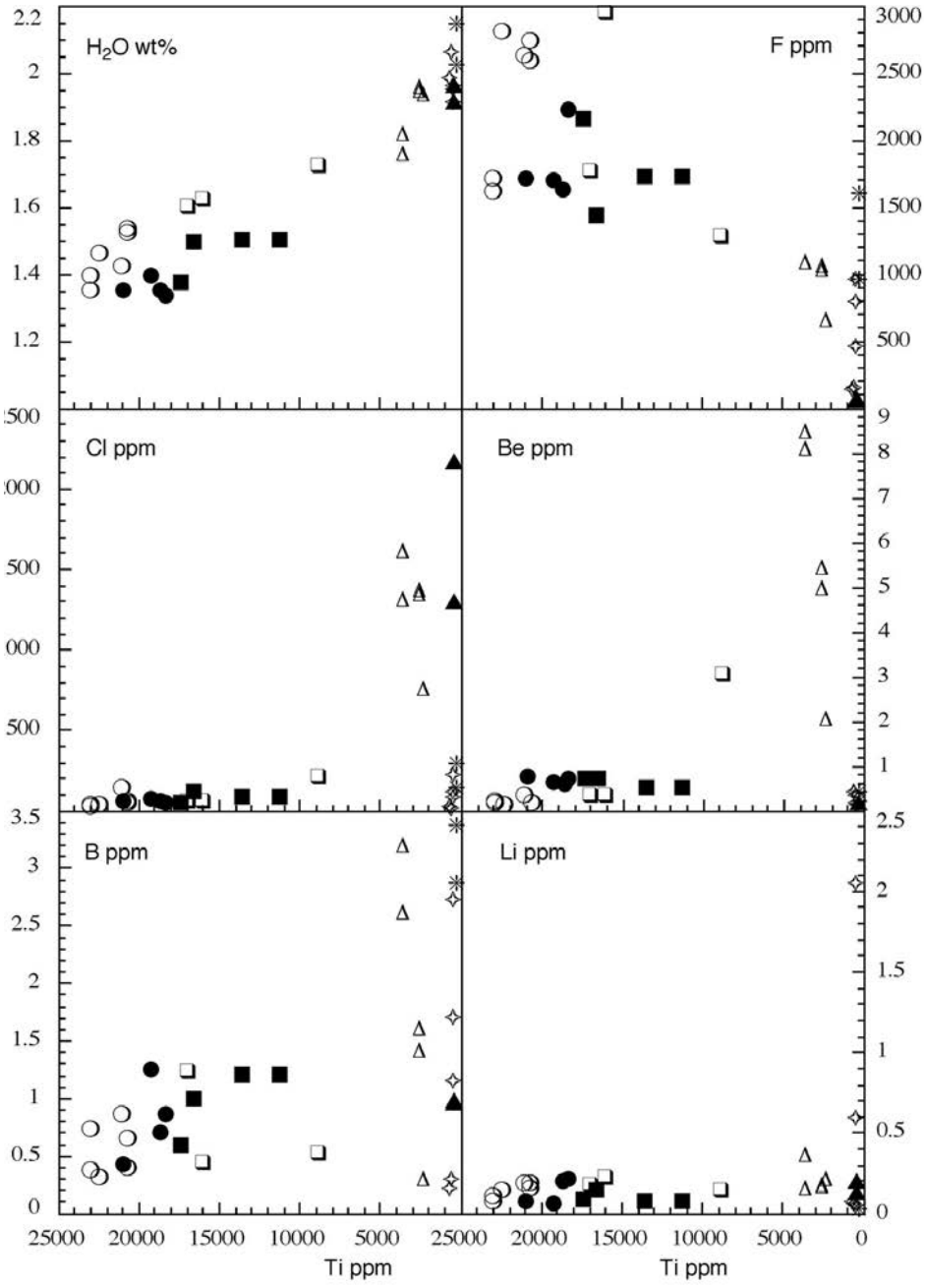

Fig. 6 - Correlations of Ti ppm vs. volatile and light elements in amphiboles. Open symbols: olivine gabbro 153 921E 3R-1 99-103. Full symbols: Fe-Ti oxide gabbro 153 921B 3R-1 33-36. Circle: red hornblendes, four samples (Cortesogno et al., 2000). Square: brown hornblendes. Triangle: green hornblendes. Diamond: actinolites. Asterisk: tremolite from olivine gabbro.

phic temperature. The progressive H_2O increase towards the lower grade and the opposite trend of F were evident. The H_2O contents lower than the stoichiometric characterised the higher-temperature red and brown hornblendes and were ascribed to important oxy-component substitution (Cortesogno et al., 2000). Average high oxy-component substitutions in amphiboles from the oxide gabbro, suggested by low H_2O and F contents, could be favoured by the rock composition. Absolute Cl values were very low in the red amphiboles (33-130 ppm) and pseudomorphic brown hornblendes (38-110 ppm), with slight increases (203 ppm) in the vein-filling brown hornblende, and low to very low (11-285 ppm) in the actinolites and tremolite. By contrast, increased Cl contents (716-2162 ppm) and pronounced compositional zoning were found in the green hornblendes. High-Cl amphiboles (Fe^{2+}-rich hastingsites, Fe-tschermakites and rarer edenites), crystallized at temperatures estimated in the range of 350°-600°C at P = 0.2–0.9 GPa, have been reported from ocean-floor metamorphosed intrusives (Honnorez and Kirst, 1975; Jacobson, 1975; Hodges and Papike, 1976; Ito and Anderson, 1983; Pritchard and Cann, 1982; Mevel, 1987; 1988; Vanko, 1986; Bideau et al., 1991), ophiolitic complexes (Liou and Ernst, 1979; Cortesogno and Lucchetti, 1984; Nehlig and Juteau, 1988), ore deposits (McCormic and McDonald, 1999) and retrogressed granulites (Markl et al., 1998). The role of the fluid phase composition and thermal evolution is discussed later.

There is little data available on the LLE of silicate minerals in MORB (e.g. Cortesogno et al., 2000). Very low Be values occur in amphiboles (Be ≤ 0.4 ppm in olivine gabbro; Be < 0.7 ppm in oxide-gabbro) except for vein-filling brown (up to 3 ppm) and green (up to 8.3 ppm) hornblendes of the olivine gabbro, where the Be is in positive correlation with the Cl. There is a broad positive correlation of Be and LREE for red (Cortesogno et al., 2000) and green hornblendes, also recorded for mantle amphiboles in equilibrium with different melt/fluid ratios (Zanetti, 1994; Zanetti et al., 2000). The Be/Nd ratios of about 0.05 were similar to those found in MORBs and OIBs (Ryan and Langmuir, 1988). At high T and P, Be is compatible with clinopyroxene, and attains values as high as 0.2-2.4 ppm in MOR differentiates, whereas in low-T hydrothermal solutions Be is nearly insoluble (Bourles et al., 1992) and values < 1 ppb are reported (Measures and Edmond, 1983). On the whole, the Be contents of pseudomorphic amphiboles probably match a predominant heritage from the pristine mineral; the higher contents in the vein-filling hornblendes of the olivine gabbro required mobilisation and precipitation from high-T fluids.

A large compositional range (0.21-3.4 ppm) arises for B in greenschist facies amphiboles and in hornblendes. The B increase from pseudomorphic actinolites to tremolite (up to 3 ppm) is consistent with the introduction of this element by hydrothermal solutions and with the composition of fluids in equilibrium with basic rocks at T ≈ 350°C (Seyfried et al., 1984). On the other hand, the wide compositional range in vein-filling green hornblendes (Fig. 4C) suggests inhomogeneous concentrations in the fluid phase. At higher metamorphic temperatures, the B content of amphiboles is generally low (0.30-1.24 ppm in titanian amphiboles; 0.43-1.20 ppm in brown hornblendes).

The greenschist facies amphiboles show a wide range of Li contents, increasing from tremolite (0.02 ppm) to actinolites (0.04-2.05 ppm). In higher T amphiboles, Li is low (0.02-0.33 ppm) with the exception of a titanian red amphibole (Li = 0.79 ppm) pseudomorphic on the clinopyroxene from the oxide gabbro (Cortesogno et al., 2000). During low-temperature (ª150°C) rock-seawater interaction in basalts, Li tends to enter secondary clay minerals (Donnelly et al., 1979; Seyfried et al. 1984, Chan et al. 1992). At greenschist facies conditions, albite and micas can preferentially host Li (Bindeman et al. 1998). On the other hand, at temperatures exceeding 350°C, Li is highly soluble in hydrothermal fluids equilibrated with tremolite–albite (Seyfried et al. 1984; 1998). Li contents of about 9 ppm have been recorded in hydrothermal fluids (Von Damm et al., 1985) comparable with 3-8 ppm in MORB (Ryan and Langmuir, 1987). Li solubility at fluid/rock ratios higher than 5 seems to yield prevailing values lower than 0.4 ppm. The Li content in the fluid phase in equilibrium with red, brown and green hornblendes, calculated as in Cortesogno et al. (2000), is generally lower than 3 ppm.

The nature of fluids

This study confirmed that hydration processes induced by diffusing fluids largely control the metamorphic reactions during brittle, transitional and, in part, ductile regimes.

The following hypotheses were considered for the origin of the fluid during the high-T ductile regime (Cortesogno et al., 2000): i) from highly evolved trapped melts (Tribuzio et al., 2000), ii) exsolution of fluids and brines from highly evolved, late-stage melts injected during tectonic-metamorphic events (Gillis, 1996; Kelley, 1997), iii) seawater-derived fluids highly modified during a long-lasting interaction with rocks at increasing metamorphic P and T (Gillis, 1996; Kelley, 1997). The origin of the fluids, mostly from seawater, during the hydrothermal and greenschist facies alteration is commonly assumed (Gillis, 1996; Kelley 1997; Fletcher et al., 1997; Scott, 1997). However a contribution by fluids originating in subsequent pulses of highly evolved MOR liquids is likely to occur at higher temperatures. For the Hess Deep gabbros, Gillis (1996) has hypothesised the prevalence of seawater-derived fluids under low-T conditions and an increasing contribution of a magmatic component at higher temperatures. Similarities in fluid compositions in evolved MOR melts are also suggested by data on amphiboles from Northern Apennine ophiolites (Tribuzio et al., 1999; 2000). In the MARK area, multiple magma injections occurred and highly evolved dioritic to trondjemitic, amphibole-bearing veins were emplaced within the plutonic sequence at temperatures comparable to those of the high temperature metamorphic event. The fluid inclusions in the igneous phases gave salinities (38-59 wt% NaCl; Kelley, 1997) and temperatures consistent with those envisaged for the fluids in equilibrium with the amphibolite facies metamorphic asssemblages. As a consequence, hydrothermal fluids associated with intrusions could play a role during the metamorphic event. Isotopic systematics able to provide data on the magmatic/seawater fluid ratio is not available at present, so only speculative rationales can be discussed. Sr isotope systematics are reported for N-MORB in late magmatic amphiboles from an oxide gabbro in Northern Apennine ophiolites, whereas slightly more radiogenic Sr in amphiboles from a diorite has been interpreted as due to chemical reactions with late fluids (Tribuzio et al., 2000). The fact that a major increase in the RE and HFS concentration would be needed during the fluid penetration of the rock to account for the composition of the amphiboles studied favours the hypothesis that the fluid originated in seawater.

The superposition of ductile, transitional and brittle fea-

tures at decreasing temperatures records the history of progressive unroofing of the gabbros from the level of liquid emplacement towards the footwall of a brittle-ductile detachment fault. The rock underwent progressive hydration at decreasing temperatures; at the same time, fluids of seawater origin penetrated the higher-temperature metamorphic zones and equilibrated chemically with the rock. Open fractures that developed during the transitional and brittle regimes in gabbros that had previously been affected by higher T processes, provided the pathway for progressive penetration of fluids of seawater origin associated with decreasing temperatures. The heat flow (Lister, 1977; 1980) as well as pressure gradients created by the opening of the fractures (Fletcher et al., 1997) provided the driving force for the fluid flows.

At shallower subseafloor conditions, fluids in contact with rock at low temperatures, even for relatively short times, are largely re-equilibrated with the rock and their composition varies greatly from that of seawater (Bideau et al., 1991; Giorgetti et al., 2001; Marescotti et al., 2000; Porter et al., 2000). Hydrothermal fluids have salinity of about 60-170% of seawater; Mg tends to have very low values and REE are about 1-3 orders of magnitude greater than seawater abundances (Michard and Albarède, 1986; Campbell et al., 1988; Scott, 1997; Bau and Dulski, 1999).

Rock/fluid equilibria cannot efficiently enrich the fluid if the $^{silicate/fluid}D_{REE,HFSE}$ >>1 (Brenan et al., 1998) is considered. During the subgreenschist and greenschist facies hydrothermal alteration, high degrees of metasomatic exchanges and important water addition to the rock from the fluid phase are implied (Fletcher et al., 1997). Moreover, elements such as Na and Mg are largely incorporated in neoblastic minerals such as chlorite and albite. On the other hand, chlorite is not able to host large amounts of REE and HFSE, so that an effective enrichment of these elements in the fluids of seawater origin is likely (Bach and Irber, 1998). The alteration of clinopyroxene to actinolite can also result in a transfer of REE and HFSE from solid to fluid. Moreover, the incorporation of water during the formation of the hydrous phases (chlorite, actinolite etc.) leads to the selective element concentration in the solutions. The “drying-up” process due to hydration reactions is known to sharply increase the concentration of most species at water/rock ratios between 10^{-1} and 10^{-2} (Reed, 1997) and represents the most important process controlling the wall rock/fluid balance.

Salinities in a range from near-seawater to six times seawater values (1-20 wt% NaCl equivalents) have been proposed for fluids penetrating the MARK gabbros at temperatures in the range 275-350°C (Kelley, 1997). The Cl contents (11-185 ppm) of greenschist facies amphiboles are consistent with high variability in hydrothermal fluids and with values generally lower than 500 ppm (Vanko, 1986). Values in the range of 100-300 ppm are considered to fit with equilibration of rocks with hydrate fluids having salinity comparable with seawater (about 3.2 wt% NaCl). Finally, the stability of the main complexing ligands such as Cl^-, F^- and OH^- can favour the permanence of REE in solution (Haas et al., 1995, Jiang et al., 1998; Bau and Dulski, 1999) and accounts for the low concentrations in greenschist facies amphiboles.

At the transition upper greenschist-lower amphibolite facies (T = 450-550°C; P = 0.2-0.3 GPa), green hornblendes have REE and HFSE contents (except for Ti) comparable with higher-T amphiboles and are characterised by an evident peak in the Cl contents. Within the same T and P range, seawater-derived fluids (0.5-20 wt% equivalent salinity) enter the vapour + liquid field and separate into CO_2-H_2O rich vapours and CO_2-H_2O-NaCl brines. A 1 wt% equivalent salinity in CO_2-H_2O vapour and a 38-59 wt% in NaCl brines has been suggested for the MARK area (Kelley, 1997). Separation and mixing of vapour and brines (Palmer, 1992) are expected to occur within the fracture net system controlled by the turbulent circulation of fluids and temperature inhomogeneities. The large Cl range (716-2162 ppm) possibly depends on equilibration with vapour and/or brines. The sharp decrease of the Cl contents in higher-T amphiboles suggests that brines are not present during amphibolite facies crystallization and that their concentrations in vapours are dramatically lowered.

The RE and HFS element enrichment in amphiboles at the greenschist - amphibolite facies transition and within the amphibolite facies could also be favoured by the decreasing stability of fluoride complexes at higher temperatures (Haas et al., 1995), and by the reduced possibility of developing chloride complexes due to the Cl separation in the brines.

CONCLUDING REMARKS

The alteration of the MARK gabbros corresponds to progressive hydration of the virtually anhydrous igneous assemblages through recrystallization at decreasing temperatures during the tectonic steps in their uplift to the seafloor. The process, largely controlled by the flow of exotic fluids, induced chemical fluxes through precipitation-dissolution mechanisms and solid-fluid reactions. Crossing the rock pile top to bottom, at lower to medium levels, during low-to-medium-T, brittle and transitional tectonic regimes, water-dominated systems developed within the fracture network, which represented the main conduit for the introduction of fluids of seawater origin. During a high-T, ductile regime, metamorphic recrystallization occurred under anhydrous to water-saturated conditions. The descent from the overlying levels of the fluid phase is responsible for the hydration process; however a contribution of late magmatic fluids exsolved from highly evolved liquids cannot be ruled out.

Evidence for rock/fluid interaction and chemical changes in the seawater-derived fluids during their descent to deeper and warmer levels can be ruled out. Deep changes are reported to affect the major and trace element composition of the seawater-derived fluids interacting with the rock under subgreenschist conditions (Bideau et al., 1991; Porter et al., 2000). During the low-T alteration of clinopyroxene to actinolite, the dissolution of RE and trace elements is prevalent, with a consequent enrichment in the fluid phase, which is antithetic to the behaviour of elements such as Mg, which enter the chlorite-actinolite bearing assemblages. In addition, an enrichment of most trace and REE elements at the expense of fluids in the solid phase is observed during the alteration of olivine to tremolite.

RE and trace element concentrations are typically lower in amphiboles that developed in cold, brittle regimes; besides the crystallographic constraints, this depends on a relatively low amphibole/water partitioning coefficient and relatively low concentrations in the fluid phase.

Be, B and Li enter amphiboles at low-medium rather than high temperatures. High F contents are restricted to higher-T amphiboles, whereas H_2O reaches values of about 2 wt% at greenschist temperatures.

On the whole, drying-up processes induced by water-

consumption reactions during subgreenschist and greenschist facies alteration could be responsible for the increased concentration of REE and trace elements that seem to characterise the fluids acting at deeper levels and higher temperatures in the rock pile.

Although the structural evidence (Fletcher et al., 1997) suggests a sharp change in the tectonic regime between the ductile and transitional events, the transition from greenschist to low-T amphibolite facies records the most significant chemical variations affecting the trace and RE elements. The high chlorine level in the amphiboles seems to have been restricted to such a transition. The vapour-NaCl brine exsolutions, which occurred approximately at the same P-T conditions, are considered responsible for the deep compositional changes and for the behaviour of the fluid phase at higher temperatures.

The remarkable increase of REE concentrations in amphiboles of the amphibolite facies is believed to depend not only on the increased element admittance to the crystal structure at higher temperatures, but also on the decreased efficiency of the chloride complexes in brine form. As gold is essentially carried in solution as a chloride complex, its precipitation in veins (Gaggero and Gazzotti, 1996), at the greenschist-amphibolite is consistent with this assumption.

At high-to-medium temperatures, pseudomorphic amphiboles have patterns similar to the clinopyroxenes they replace, thus implying a prevalent heritage, but some element introduction by fluids (mainly LREE and Nb) can also be envisaged. Element mobilisation on a small scale is also suggested by the compositional changes observed in amphiboles that developed by reactions involving plagioclase and/or oxides. Such low diffusivity is consistent with the lowered water/rock ratios and the water/amphibole partitioning coefficient. The geochemical similarity between the HT, titanian amphiboles (Cortesogno et al., 2000) and amphibolite-facies pseudomorphic hornblendes suggests equilibrium with compositionally homogeneous fluids within the rock-dominated systems.

Vein-filling amphiboles display similar patterns, characterised by negative Sr, Zr, Eu Ti anomalies, which likely reflect comparable compositions to the fluids circulating in the veins/fractures. The reactions involving the wall-rock mineral phases within fractures imply a rock/fluid element exchange; however the precipitation of the vein-filling mineral phase seems to be the prevailing process and resulted in an element gain in the rock balance. Fractures are sutured by centripetal symmetric precipitation of plagioclase and hornblende as major phases. The $^{solid/fluid}D_{REE, HFSE} >> 1$ (Brenan et al., 1998) implies the progressive dilution of the fluid phase. As a consequence, a centripetal mineral and compositional zoning can develop if the supply from large-scale circulation stops.

The inter-intragranular diffusion from the joints to the wall rock, responsible for the kinetic of the metastable igneous remnants (olivine, pyroxenes), highlights the transition from anhydrous to water-saturated conditions controlled by fluid-diffusion and by fluid-consumption reactions.

ACKNOWLEDGEMENTS

This research was funded by Genoa University funds for L. Cortesogno. The critical reading by Paola Tartarotti (Milan University) is warmly acknowledged.

REFERENCES

Alt J., 1995. Subseafloor processes in Mid-Ocean ridge hydrothermal processes. In: S.E. Humphris, R.A. Zierenberg, L.S. Mullineaux, R.E. Thomson (Eds.), Seafloor hydrothermal systems: physical, chemical biological and geological interactions. AGU Monograph, 91: 85-114.

Anders E. and Ebihara M., 1982. Solar system abundances of the elements. Geochim. Cosmochim. Acta, 46: 2363-2380.

Bach W. and Irber W., 1998. Rare earth element mobility in the oceanic lower sheeted dyke complex: evidence from geochemical data and leaching experiments. Chem. Geol., 151 (1-4): 309-326.

Barling J., Hertogen J., and Weis D., 1997. Whole-rock geochemistry and Sr-, Nd-, and Pb-isotopic characteristics of undeformed, deformed, and recrystallized gabbros from Sites 921, 922, and 923 in the MARK area. In: J.A. Karson, M. Cannat, D.J. Miller, D. Elthon (Eds.), Proceed. ODP, Sci. Results, 153: 351-362.

Bau M. and Dulski P., 1999. Comparing yttrium and rare earths in hydrothermal fluids from the Mid-Atlantic Ridge: implications for Y and REE behavior during near-vent mixing and for the Y/Ho ratio of Proterozoic seawater. Chem. Geol., 155 (1-2): 77-90.

Bideau D., Hebert R., Hekinian R. and Cannat M., 1991. Metamorphism of deep seated rocks from the Garret Ultrafast Transform (East Pacific Rise near 13° 25' S). J. Geophys. Res., 96: 10079-10099.

Bindeman I.N., Davis A.M. and Drake M.J., 1998. Ion microprobe study of plagioclase-basalt partition experiments at natural concentration levels of trace elements. Geochim. Cosmochim. Acta, 62 (7): 1175-1193.

Blundy J.D. and Wood B.J., 1994. Prediction of crystal-melt partition coefficients from elastic moduli. Nature, 372: 452-454.

Bourles D.L., Brown E.T., Raisbeck G.M., Yiou F. and Gieskes J.M., 1992. Beryllium isotope geochemistry of hydrothermally altered sediments. Earth Planet. Sci. Lett., 109: 47-56.

Brenan J.M., Neroda E., Lundstrom C.C., Shaw H.F., Ryerson F.J. and Phinney D.L., 1998. Behavior of boron, beryllium, and lithium during melting and crystallization: constraints from mineral-melt partitioning experiments. Geochim. Cosmochim. Acta, 62 (12): 2129-2141.

Campbell A.C., Bowers T.S. and Edmond J.M. 1988. A time series of vent fluid composition from 21°N, EPR (1979, 1981 and 1985) and the Guayamas Basin, Gulf of California (1982, 1985). J. Geophys. Res., 93: 4537-4549.

Cannat M., Ceuleneer G. and Fletcher J., 1997. Localization of ductile strain and the magmatic evolution of gabbroic rocks drilled at the Mid-Atlantic Ridge (23°N). In: J.A. Karson, M. Cannat, D.J. Miller, D. Elthon (Eds.), Proceed. ODP, Sci. Results, 153: 77-98.

Cannat M., Mével C., Maia M., Deplus C., Durand C., Gente P., Agrinier P., Belarouchi A., Dubuisson G., Humler E. and Reynolds J., 1995. Thin crust, ultramafic exposures, and rugged faulting patterns at the Mid-Atlantic Ridge (22°-24°N). Geology, 23 (1): 49-52.

Casey J.F., 1997. Comparison of major- and trace element geochemistry of abyssal peridotites and mafic plutonic rocks with basalts from the MARK region of the Mid-Atlantic Ridge. In J.A. Karson, M. Cannat, D.J. Miller, D. Elthon (Eds.), Proceed. ODP, Sci. Results, 153: 181-241.

Chan L.H., Edmond J.M., Thompson G. and Gillis K., 1992. Lithium isotopic composition of submarine basalts: implications for the lithium cycle in the oceans. Earth Planet. Sci. Lett., 108: 151-160.

Cortesogno L. and Lucchetti G., 1984. Ocean floor metamorphism of the volcanic and sedimentary sequences in the Northern Apennine ophiolites: Mineralogical and paragenetic features. Ofioliti, 9: 363-400.

Cortesogno L., Gaggero L., and Zanetti A., 2000. Rare earth and trace elements in igneous and high temperature metamorphic

minerals of oceanic gabbros (MARK area, Mid-Atlantic Ridge). Contrib. Mineral. Petrol., 139: 373-393.

Cortesogno L., Gianelli G. and Piccardo G.B., 1975. Pre-orogenic metamorphic and tectonic evolution of the ophiolite mafic rocks (Northern Apennine and Tuscany). Boll. Soc. Geol. It., 94: 291-327.

Donnelly T.W., Pritchard R.A. Emmerman R. and Puchelt H., 1979. The aging of oceanic crust: synthesis of mineralogical and chemical results of DSDP Legs 51-53. Init Repts DSDP, 51-53, part 2: 1563-1577,.

Ernst W.G. and Liu J., 1998. Experimental phase-equilibrium study of Al and Ti contents of calcic amphibole in MORB – A semiquantitative thermobarometer. Am. Mineral., 83 (9-10): 952-969.

Fletcher J.M., Stephens C.J., Petersen E.U., Skerl L., 1997. Greenschist facies hydrothermal alteration of oceanic gabbros: a case study of element mobility and reaction paths. In J.A. Karson, M. Cannat, D.J. Miller, D. Elthon (Eds.), Proceed. ODP, Sci. Results, 153: 389-398.

Gaggero L. and Cortesogno L., 1997. Metamorphic evolution of oceanic gabbros: recrystalization from subsolidua to hydrothermal conditions in the MARK area (ODP Leg 153). Lithos, 40: 105-131.

Gaggero L., and Gazzotti M., 1996. Primary and secondary oxides, sulfides and accessory minerals in Mid-Atlantic gabbros: mineralogy and petrology. Ofioliti, 21 (2): 105-116.

Gillis K.M., 1996. Rare earth element constrains on the origin of amphibole in gabbroic rocks from Site 894, Hess Deep. In: C. Mével, K.M. Gillis, J.F. Allan, P.S. Meyer (Eds.), Proceed. ODP, Sci. Results, 147: 59-75.

Gillis K.M., Thompson G. and Kelley D.S. 1993. A view of the lower crustal component of hydrothermal systems at the Mid-Atlantic Ridge. J. Geophys. Res. 98 (B11): 19597-19619.

Giorgetti G., Marescotti P., Cabella R. and Lucchetti G., 2001. Clay minerals mixtures as alteration products in pillow basalts from the eastern flank of the Juan de Fuca Ridge: a TEM-AEM study. Clay Minerals, 36: 75-91.

Haas J.R., Shock E.R. and Sassani D.C., 1995. Rare earth elements in hydrothermal systems: estimate of standard partial molal thermodynamic properties of aqueous complexes of the rare earth elements at high pressures and temperatures. Geochim. Cosmochim. Acta, 59: 4329-4350.

Hodges F.N. and Papike J.J., 1976. DSDP site 344: magmatic cumulates from oceanic layer 3. J. Geophys. Res., 81: 4135-4151.

Honnorez J. and Kirst P., 1975. Petrology of rodingites from the equatorial Mid-Atlantic fracture zones and their geotectonic significance. Contrib. Mineral. Petrol., 49: 233-257.

Ito E. and Anderson A.T., 1983. Submarine metamorphism of gabbros from the Mid-Cayman Rise: petrographic and mineralogic constraints on hydrothermal processes at slow spreading ridges. Contrib. Mineral. Petrol., 82: 371-388.

Jacobson S.S., 1975. Dashkesanite: high-chlorine amphibole from St. Paul's rock, equatorial Atlantic and Transcaucasia, USSR. Smithson. Contrib. Earth Sci., 14: 17-20.

Jiang J., Ozaki T., Machida K. and Adachi G., 1998. The characteristics of chemical vapour transport and mutual separation for the scandium, yttrium and lanthanum mediated by the corresponding gaseous rare earth chloride complexes. J. Alloys and Compounds, 264: 157-163.

Karson J.A., Cannat M., Miller D.J. and Elthon D. (Eds.,) 1997. Proc. ODP Sci. Results 153: College Station, TX (Ocean Drilling Program).

Kelley D.S., 1997. Fluid evolution in slow-spreading environment. In J.A. Karson, M. Cannat, D.J. Miller, D. Elthon (Eds.), Proceed. ODP, Sci. Results, 153: 399-415.

Kempton P.D. and Hunter A.G., 1997. A Sr-, Nd-, Pb-, O-isotope study of plutonic rocks from MARK, Leg 153: implications for mantle heterogeneity and magma chamber processes. In J.A. Karson, M. Cannat, D.J. Miller, D. Elthon (Eds.), Proceed. ODP, Sci. Results, 153: 305-319.

Leake B.E., Wolley A.R., Arps C.E.S., Birch W.D., Gilbert M.C., Grice J.D., Hawthorne F.C., Kato A., Kish H., Krivovichev V.G., Linthout K., Laird J., Mandarino J.A., Maresch W.V., Nickel E.H., Rock N.M.S., Schumacher J.C., Stephenson N.C.N., Ungaretti L., Whittaker E.J.W. and Youzhi G., 1997. Nomenclature of amphibole: report of the subcommittee on amphiboles of the International Mineralogical Association, Commission on new minerals and mineral names. Canad. Mineral., 35: 219-246.

Liou J.G. and Ernst W.G., 1979. Oceanic ridge metamorphism of the East Taiwan Ophiolite. Contrib. Mineral. Petrol., 68: 335-348.

Liou J.C., Kuniyoshi and Ito K. 1974. Experimental studies of the phase relations between greenschist and amphibolite in a basaltic system. Am. J. Sci., 274: 613-632.

Lister C.R.B., 1977. Qualitative models of spreading-center processes including hydrothermal penetration. Tectonophysics, 37: 203-218.

Lister C.R.B., 1980. Heat flow and hydrothermal circulation. Ann. Rev. Earth Planet Sci., 8: 95-117.

Marescotti P., Vanko D.A. and Cabella R., 2000. From oxidizing to reducing alteration: mineralogical variations in pillow basalts from the East Flank, Juan de Fuca Ridge. In: A. Fischer, E.E. Davis, C. Escutia (Eds.), Proceed. ODP Sci. Results, 168: 119-136

Markl G., Ferry J. and Bucher K., 1998. Formation of saline brines and salt in the lower crust by hydration reactions in partially retrogressed granulites from the Lofoten Islands, Norway. Am. J. Sci., 298 (9): 705-757.

McCormic K.A. and McDonald A.M., 1999. Chorine-bearing amphiboles from the Fraser mine, Sudbury, Ontario, Canada: description and crystal chemistry. Canad. Mineral., 37 (6): 1385-1403.

Measures C.I. and Edmond J.M., 1983. The geochemical cycle of ^{9}Be: a reconnaissance. Earth Planet. Sci. Lett., 66: 101-110.

Mével C., 1987. Evolution of oceanic gabbros from DSDP Leg 82: influence of the fluid phase on metamorphic crystallizations. Earth Planet. Sci. Lett., 83: 67-79.

Mével C., 1988. Metamorphism of oceanic layer 3, Gorringe Bank, eastern Atlantic. Contrib. Mineral. Petrol., 100: 496-509.

Michard A. and Albarede F., 1986. The REE content of some hydrothermal fluids. Chem. Geol., 55: 51-60.

Nehlig P. and Juteau T., 1988. Flow, porosities, permeabilities and preliminary data on fluid inclusions and fossil thermal gradients in the crustal sequence of the Semail ophiolite (Oman). Tectonophysics, 151: 199-221.

Palmer M.R., 1992. Controls over the chlorine concentrations of submarine hydrothermal vent fluids evidence from Sr/Ca and ^{87}Sr/^{86}Sr ratios. Earth Planet. Sci. Lett., 109: 37-46.

Porter S., Vanko D.A. and Ghazi A.M., 2000. Major and trace element compositions of secondary clays in basalts altered at low temperature, eastern flank of the Juan de Fuca Ridge. In: A. Fischert, E.E. Davis, C. Escutia (Eds.), Proceed. ODP Sci Results, 168: 149-157

Prichard H.M. and Cann J.R., 1982. Petrology and mineralogy of dredged gabbro from Gettysburg bank, Eastern Atlantic. Contrib. Mineral. Petrol., 79: 46-55.

Reed M.H., 1997. Hydrothermal alteration and its relationships to ore fluid composition. In: H.L. Barnes (Ed.), Geochemistry of hydrothermal ore deposits. Wiley & Sons, p. 303-365.

Ross K. and Elthon D., 1997. Cumulus and post-cumulus crystallization in the oceanic crust: major-and trace-element geochemistry of Leg 153 gabbroic rocks. In J.A. Karson, M. Cannat, D.J. Miller, D. Elthon (Eds.), Proceed. ODP, Sci. Results, 153: 333-350.

Ryan J.G. and Langmuir C.H., 1987. The systematics of lithium abundances in young volcanic rocks. Geochim. Cosmochim. Acta, 51: 1727-1741.

Ryan J.G. and Langmuir C.H., 1988. Beryllium systematics in young volcanic rocks; implications for ^{10}Be. Geochim. Cosmochim. Acta, 52: 237-244.

Scott S.D., 1997. Submarine hydrothermal systems and deposits. In: H.L. Barnes (Ed.), Geochemistry of hydrothermal ore deposits. Wiley & Sons, p. 797-875.

Seyfried W.E., Janecki D.R. and Mottl M.J., 1984. Alteration of the oceanic crust: implication for geochemical cycles of lithium and boron. Geochim. Cosmochim. Acta, 48: 557-569.

Seyfried W.E., Chen X. and Chan L.H., 1998. Trace element mobility and lithium isotope exchange during hydrothermal alteration of seafloor weathered: an experimental study at 350°C, 500 bars. Geochim. Cosmochim. Acta, 62: 949-960.

Shipboard Scientific Party, 1995. Proceed. ODP Initial Repts., 153.

Staudigel H., Yayanos A., Chastain R., Davies G., Verdurmen E.A.T., Schiffman P., Bourcier R. and De Baar H., 1998. Biologically mediated dissolution of volcanic glass in seawater. Earth Planet. Sci. Lett., 164 (1-2): 233-244.

Tribuzio R., Tiepolo M., Vannucci R. and Bottazzi P., 1999. Trace element distribution within olivine-bearing gabbros from the Northern Apennine ophiolites (Italy): evidence for post-cumulus crystallization in MOR-type gabbroic rocks. Contrib. Mineral. Petrol., 134: 123-133.

Tribuzio R., Tiepolo M. and Thirwall M., 2000. Origin of titanian pargasite in gabbroic rocks from the Northern Apennine ophiolites (Italy): insights into the late magmatic evolution of a MOR-type intrusive sequence. Earth Planet. Sci. Lett., 176: 281-293.

Vanko D.A., 1986. High chlorine amphibole from oceanic rocks; product of highly saline hydrothermal fluids? Amer. Mineral., 71: 51-59.

Vanko D.H. and Laverne C., 1998. Hydrothermal anorthitization of plagioclase within the magmatic/hydrothermal transition at mid-ocean ridges: examples from deep sheeted dikes (Hole 504B, Costa Rica Rift) and a sheeted dike root zone (Oman ophiolite) Earth Planet. Sci. Lett., 162 (1-4): 27-43.

Von Damm K.L., Edmond J.M., Grant G., Measures C.I., Walden B. and Weiss R.F., 1985. Chemistry of submarine hydrothermal solutions at 21°N, East Pacific Rise. Geochim. Cosmochim. Acta, 49: 2197-2220.

Zanetti A., Oberti R., Piccardo G.B. and Vannucci R., 2000. Light lithophile (Li, Be and B), volatile (H, F and Cl) and trace element composition of mantle amphiboles from Zabargad peridotite: insights into the multistage subsolidus evolution of subcontinental mantle during Red Sea rifting. Goldschmidt 2000, Jour. Conf. Abs., 5 (2): 1120.

Zanetti A., 1994. Ruolo cristallochimico degli elementi maggiori e minori nei minerali delle associazioni ultrafemiche del mantello. Unpubl. PhD Thesis, Univ. Pavia, 237 pp.

Received, March 24, 2003
Accepted, January 15, 2004

APPENDIX

Sample 153 921E 3R-1 99-103 Olivine-gabbro

Coarse grained with euhedral plagioclase (40%, grain size between 0.5-6 mm) and subhedral olivine (> 10%). Large anhedral clinopyroxene (> 10%, grain size between 3-6 mm) often includes plagioclase grains. Ilmenite (≥ 1%) occurs as micro-inclusions at the rims of the clinopyroxene, or as small interstitial grains. Tiny sulphide inclusions occur in the plagioclase and, more rarely, in the clinopyroxene. Gneissic bands (thickness 0-5 mm) with granoblastic plagioclase and clinopyroxene cut the rock. The development of granoblastic bands is progressive, with local concentrations of pyroxene and red amphibole (maximum grain size: 0.5 mm). Porphyroclastic plagioclase, clinopyroxene and olivine relics occur within the granoblastic plagioclase, clinopyroxene and red amphibole (< 1%, average grain size: 0.5 mm). Zoned brown amphibole (ª6% in volume) diffuses in the rock from microcracks cutting the foliation. Olivine (2-3 mm) is completely replaced by tremolite and chlorite (Trm + Tc + Chl ª 18%). Later microcracks are filled by green hornblende (ª 2% in volume), oligoclase, actinolite, chlorite, albite, and titanite.

Sample 153 921B 3R-1 33-36 Oxide gabbro

The rock is medium-grained, with subhedral plagioclase (ª40% in volume, grain size 1-4 mm) and clinopyroxene (ª40% in volume, grain size 1-4 mm), and trellis texture exsolutions of ilmenite and Ti-magnetite (13-14% in volume; 1-2 mm). Apatite (£1% in volume), minor chalcopyrite and pyrrothite are accessory phases.

The porphyroclastic igneous phases are wrapped in granoblastic plagioclase, clinopyroxene, orthopyroxene, red amphibole (5-7% in volume), ilmenite and Ti-magnetite (13-14% in volume; grain size 1-2 mm). The brown amphibole developed along microfractures replacing pyroxene and red amphibole; green hornblende occurs filling later fractures and propagating in the rock. Modal brown and green amphibole is ≈ 4%.